SRL-3-F-2001

ALL-SOLID-STATE DRIVERS FOR HIGH POWER EXCIMER LASERS USED IN PROJECTION GAS IMMERSION LASER DOPING

Prepared by

Dr. Jonah Jacob

Science Research Laboratory, Inc.
15 Ward Street
Somerville MA 02143

PHASE II FINAL TECHNICAL REPORT

Contract Number MDA972-97-C-0044

DARPA Order No. F554

Program Code No. 7D10

September 2, 1997 to February 28, 2001

Prepared for

This material is based upon work supported by the
Defense Advanced Research Projects Agency
Electronics Technology Office
3701 North Fairfax Drive
Arlington VA 22203 1714

September 25, 2001

REPORT DOCUMENTATION PAGE

Form Approved
OMB No. 0704-0188

1. AGENCY USE ONLY *(Leave blank)*	2. REPORT DATE	3. REPORT TYPE AND DATES COVERED
	09/25/01	Final 09/02/97 to 02/28/01

4. TITLE AND SUBTITLE
ALL-SOLID-STATE DRIVERS FOR HIGH POWER EXCIMER LASERS USED IN PROJECTION GAS IMMERSION LASER DOPING

5. FUNDING NUMBERS

6. AUTHOR(S)
DR JONAH JACOB

7. PERFORMING ORGANIZATION NAME(S) AND ADDRESS(ES)

SCIENCE RESEARCH LABORATORY INC
15 WARD ST., SOMERVILLE, MA 02143

8. PERFORMING ORGANIZATION REPORT NUMBER
3 - F - 2001

9. SPONSORING/MONITORING AGENCY NAME(S) AND ADDRESS(ES)
Defense Advanced Research Projects
Agency Contracts Management Office
3701 North Fairfax Dr
Arlington VA 22203 1714

10. SPONSORING/MONITORING REPORT NUMBERS
MDA972-97-C-0044

11. SUPPLEMENTARY NOTES

12a. DISTRIBUTION/AVAILABILITY STATEMENT

UNLIMITED DISTRIBUTION

12b. DISTRIBUTION CODE

13. ABSTRACT *(Maximum 200 words)*

The objective of this SBIR program is to develop all-solid-state pulsed modulators to drive the high power excimer lasers required to commercialize the Projection Gas Immersion Laser Doping (P-GILD) process. P-GILD uses a pulsed, 200-watt-class excimer laser as an illumination source to produce ultra-shallow, low-sheet resistance, box-like and retrograde impurity profiles in silicon without the use of high temperature anneals or conventional ion implantation. P-GILD thus meets all of the criteria for fabricating optimized deep-submicron devices. The P-GILD process requires a factor-of-20 scale up in average power from the production-worthy excimer laser technology now developed for 0.25 micron DUV lithography. All-solid-state drivers were essential to meeting component lifetime and cost of ownership requirements in the 10 watt KrF lasers used in DUV lithography and solid state drivers will be even more important in developing the high power excimer laser required for P-GILD. In this SBIR, SRL worked closely with Cymer, the leading supplier of excimer lasers for DUV lithography worldwide, and Ultratech Stepper, the developer of the P-GILD process, to generate a detailed engineering design of an all-solid-state driver for a high power excimer laser designed to meet P-GILD process requirements. In addition, an all-solid-state driver was fabricated to test critical aspects of the design on a 150 watt excimer laser head supplied by Cymer.

14. SUBJECT TERMS
Silicon Controlled Rectifier, Magnetic Switch, XeCl Laser, XeF Laser, Pulsed Power, Semiconductor Manufacturing, Integrated Circuit

15. NUMBER OF PAGES
54

16. PRICE CODE

17. SECURITY CLASSIFICATION OF REPORT	18. SECURITY CLASSIFICATION OF THIS PAGE	19. SECURITY CLASSIFICATION OF ABSTRACT	20. LIMITATION OF ABSTRACT
UNCLASSIFIED	UNCLASSIFIED	UNCLASSIFIED	UNCLASSIFIED

I. INTRODUCTION

DARPA is making a significant investment in the development of Projection Gas Immersion Laser Doping for the production of ultra-shallow junction, low power ICs. P-GILD uses a pulsed 200 watt XeCl laser at 308 nm as an illumination source to produce ultra-shallow, low-sheet-resistance, box-like and retrograde impurity profiles in silicon without the use of high temperature anneals or conventional ion implantation. In so doing, P-GILD meets all of the criteria for fabricating optimized deep-submicron devices. In addition, the equipment technology is vacuum-compatible, single-wafer and modular. Doping occurs from the gas-phase in a process that is activated by nanosecond thermal cycles induced in the silicon by absorption of the excimer laser light. Rather than using photoresist or thin-film layers to mask undoped regions from impurities, P-GILD utilizes a chromeless reticle to pattern the excimer laser beam and limit the extent of the thermal process. Once patterned, the beam is projected onto the wafer with diffraction-limited optics. In this manner, P-GILD eliminates the numerous steps and attendant equipment costs associated with the mask formation and removal process. Finally, like step-and-repeat lithography, P-GILD is performed field by field across the wafer.

P-GILD has many advantages over conventional ion implantation doping including

(1) Direct Compatibility with Low Cost Minifabs: Tool modularity exhibited by direct compatibility with single-wafer processing modules arranged in clusters for production of lower volume custom and semi-custom ICs

(2) Process Simplification: To adapt ion implantation to emerging deep-submicron linewidths, multiple process steps and stringent process controls are needed. Wafer charging, crystal damage, photoresist burning, ion sputtering, and dopant activation will add to the complexity of the ion beam process (Figure 1). Moreover, mask formation and removal steps add significantly to the cost, contamination and complexity of the overall process. For the high-dose source/drain process, P-GILD reduces the doping sequence by more than 10 steps and, more importantly, replaces the lithotool, ion implanter, plasma asher, and rapid thermal or furnace annealing tool, yielding significant savings in overall process cost as well as a factor-of-5 reduction in footprint.

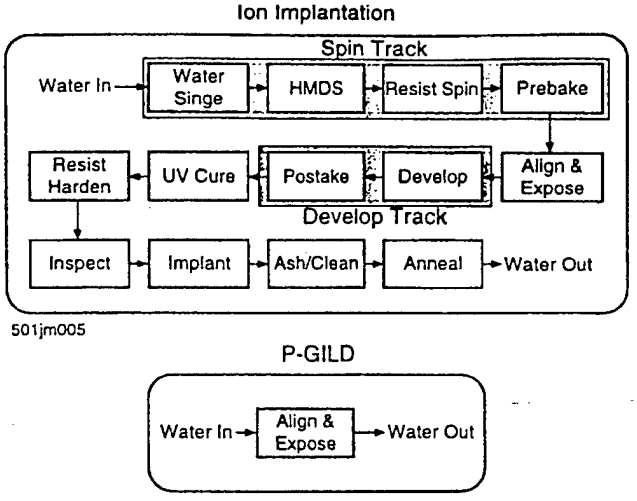

Figure 1: Comparison of Selective Doping Sequences for P-GILD and Ion Implantation

For shallow junction formation, Projection Gas Immersion Laser Doping represents a truly innovative approach. The excimer-laser-based technique merges gas-phase diffusion, thermal annealing, and deep-UV projection lithography into a single technology to produce junctions that exhibit the following characteristics.

1. Ultrashallow junction depth - demonstrated junction depths down to 10 nm extends technology to 0.1 micron device generation

2. Optimized deep-submicron impurity profiles - box-like, supersaturated, zero-gate-overlap source/drain profiles eliminate parasitic components of resistance and capacitance and minimize intrinsic sheet resistance of the layers.

3. Room temperature processing - excimer-laser-induced, junction-localized nanosecond thermal cycles eliminate temperature cycles in the bulk silicon and defect generation caused by thermal annealing.

The ultimate viability of the P-GILD process will depend on achieving high throughput and economically viable process costs. In order to meet P-GILD process throughput requirements, the P-GILD excimer laser system will have to operate at an average power of 200 watts. This average power can be achieved at a single pulse energy of 0.5 Joules and a pulsed repetition rate of 400 pulses per second. A 200 watt XeCl laser operating at 308 nm was considered baseline, although development of an XeF laser (351 nm) for this application was discussed with Cymer and Ultratech. Breadboard testing was performed on a 0.5 Joule/ pulse, 250 pulse per second, KrF laser (248 nm).

Currently the 200 watt XeCl lasers available from Lambda Physik and other suppliers have neither the component lifetime nor reliability to affordably provide the UV laser beams needed for P-GILD. These existing laser devices are not production-worthy, having an annual cost of ownership of more than $900K, and a MTBR of less than 1 billion shots (which is less than 1 month of continuous operation at a pulse rate of 400 pulses per second). In fact, production-worthy KrF laser systems are only now just becoming available at the 10 watt average power level needed to meet requirements imposed by 0.25 micron DUV lithography. These KrF lasers, which are powered with all-solid-state pulsed drivers furnished exclusively by SRL, are now being sold commercially in large numbers to stepper manufacturers such as Nikon, Canon, ASML and SVG-L by Cymer, Inc. The development of production-worthy 10 watt KrF lasers for lithography provides critical insights into the problems which must be faced in developing the 200 watt excimer laser required for P-GILD.

All discharge-pumped excimer lasers currently on the market are powered with thyratron-based pulsed drivers -- the sole exception is the 10 watt KrF laser developed by Cymer for DUV lithography. The thyratrons in these circuits have proven to have an operating life of less than 1 billion shots when used to drive the highly inductive, nonlinear load characteristic of excimer laser discharges at 0.5 Joules per pulse and 400 pulses per second. Consequently, the thyratrons would have to be replaced approximately every month at a cost of more than $25K.

Another critical lifetime issue and cost driver in these laser systems is related to erosion of the metal discharge electrodes due to late time discharge arcs. Excimer laser discharges are inherently unstable because multi-step ionization processes dominate the discharge. Consequently, excimer laser discharges are stable in the desired spatially uniform glow regime for only 40 to 50 nsec before the discharge collapses spatially into a late time arc. The energy remaining in the discharge circuit is then deposited locally at the arc attachment points on the electrode surface -- which are typically less than 1 mm in diameter. So on each pulse, material is eroded from each of the two electrode surface. The stability of these discharges is an extremely strong function of the details of the electrode shape or profile. After less than 2 mm of the electrode surface is eroded, the electrodes have to be replaced, because the transition from uniform glow discharge to arc is occurring sooner and sooner in the discharge pulse and decreasing the single pulse laser energy and average power of the laser.

For the 10 watt KrF lasers used in DUV lithography, the single pulse energy is less than 10 mJ. Even for this laser, however, with a thyratron-based driver, the electrodes had to be replaced every 2 billion shots, or after every 3 weeks of continuous operation. Although careful statistical data has not yet been obtained for the 200 watt thyratron-switched Lambda Physik XeCl laser currently being used at Ultratech in the P-GILD program, it is expected that the lifetime of its electrodes will be significantly less than 1 billion shots since the single pulse energy input in this laser is 20 times the single pulse energy input in the 10 watt KrF laser used in DUV lithography. Replacement of the discharge electrodes would have to be performed after every month of continuous operation. For a laser of this power level, electrode replacement is estimated to cost approximately $50K.

In addition to the issues described above, as the electrode material erodes, the eroded metal vapor reacts with the halogen-bearing molecules in the laser gas and creates a need to process the laser gas every 200 million shots and to replenish the halogen-bearing gas -- which also adds to the operating expense of the laser.

If just the cost of replacing the thyratron and the discharge electrodes is considered, the operating cost of a 200 watt XeCl laser will be more than $900K per year. When the $500K laser capital cost is included over a 5 year amortization period, the total annual cost of ownership for this 200 watt XeCl system can easily exceed $1000K. In the case of the 10 watt KrF laser used in DUV lithography, the total operating cost of the thyratron-switched laser system was $250K per year, dominated primarily by the cost of the replacement thyratrons and the replacement electrodes. With the SRL all-solid-state driver, the annual operating cost for this 10 watt KrF laser has been reduced to approximately $50K.

These cost reductions were obtained in three ways. First, all-solid-state drivers using Silicon Controlled Rectifiers (SCRs) were employed as the primary commutator and not thyratrons. SCRs have demonstrated a 100-fold shot life advantage over thyratrons. This means that a single SCR has a lifetime of 2×10^{11} shots or more than 6 years of continuous operation at 1000 pulses per second. The direct result is that the pulsed power unit will never have to be repaired over the life of the tool. Secondly, the SRL all-solid-state driver contains energy recovery circuits which recover the energy stored in the discharge circuit just after the laser pulse terminates and just before the formation of the localized arc which erodes the discharge

electrodes. With this unique energy recovery circuit, the electrode lifetime has been extended significantly in the 10 watt KrF laser manufactured by Cymer for lithography. Finally, with greatly diminished electrode erosion, the excimer laser gas lifetime is also extended. All of these critical improvements resulted in a fivefold reduction in annual cost of ownership.

With the 200 watt excimer laser required for P-GILD, the successful design of an all-solid-state driver will be even more critical. With the twenty-fold increase in laser output power, the electrode and gas life issues discussed above are much exacerbated, especially since material damage is a highly nonlinear process. Energy recovery circuits that greatly reduce the fraction of discharge energy deposited in the electrodes will have to be developed at the required 20 times higher average power. At these higher powers, multiple SCRs at the front end of the discharge circuit will have to be arrayed in parallel to switch the increased energy. Fortunately SRL has already developed branched magnetic front ends to allow SCRs to operate safely in parallel at the required pulse rates.

The key to the development of a high power excimer laser having an affordable annual operating cost (and cost of ownership) is the development of an all-solid-state pulsed power driver with energy recovery circuits and a branched magnetic front end.

II. TECHNICAL OBJECTIVES

The use of excimer lasers operating with high current, transverse, atmospheric discharges has sparked new interest in improving the reliability of the associated pulsed drivers. In the past, these modulators were based on thyratron or spark-gap-based technology. This rather primitive technology exhibited three major drawbacks. First, the modulator was short-lived leading to high cost of ownership. Second, the lack of control over the discharge waveform led to an inefficient discharge and late time arcing. The result of this was increased electrode erosion and an even higher cost of ownership. Finally, the performance of the thyratron or spark gap switching elements were not repeatable causing pulse-to-pulse variation in the laser output.

SRL all-solid-state drivers are based on silicon-controlled-rectifiers (SCRs) and insulated-gate, bipolar transistors (IGBTs) combined with nonlinear magnetic pulse compression technology. The all-solid-state driver technology to be used in this effort was originally developed to power copper vapor lasers in the Atomic Vapor Laser Isotope Separation (AVLIS) program at Lawrence Livermore National Laboratory (LLNL). At LLNL, these drivers have been operated with 30 nsec pulse durations and have achieved 3 X 10^{11} shot life in continuous operation at 4400 pulses per second.

These all-solid-state drivers require only a 1000 VDC power source to charge the primary energy storage capacitors and TTL level input trigger pulses. The energy from a DC power source is transferred to the primary storage capacitors by an IGBT and then commutated to form pulses with a 25 μsec duration. These pulses are then temporally compressed with high efficiency by successive stages of magnetic pulse compression. Four stages of pulse compression are typically required to obtain the 120 nsec pulses needed to charge the peaking capacitors at the output stage. The final $\leq$28 kV output pulse is formed with a fractional-turn

output transformer which then charges the peaking capacitors. Self-breaking of the discharge transfers the energy in the peaking capacitors to the discharge.

These drivers are modular and feature a branched magnetic front end and utilize the fractional-turn output transformer to add the outputs from each module. These features insure that the driver can be made compact, since the only locations at which voltage above 1 kV appears is on the output transmission line which connects the fractional-turn output transformer to the final pulse compression stages and to the peaking capacitors at the plasma discharge tube.

The branched front end protects the solid state commutator against energy reflected from the time-varying discharge load and insures that the safe operating envelope for the solid state switches can never be exceeded even with the sometimes pathological load conditions presented by these laser plasma discharges. Each parallel branch is sized so that semiconductors can handle all of the energy in that branch under any fault mode condition. The fractional-turn transformer is the key to modularity and is used to add the voltage from each of the branches at the output of the individual commutated pulse compression modules. This feature allows an extremely compact, highly reliable design since most of the circuit operates at a maximum voltage of 1 kV with the 25 kV output voltage appearing only at the output of the fractional-turn transformer, at the final output compression stages and at the peaking capacitors.

As stated above, all-solid-state driver technology was originally developed to power copper vapor lasers at LLNL. LLNL has extensively tested these drivers at 4400 pps with the rapidly time varying, highly inductive loads represented by the longitudinal copper vapor laser discharge. This discharge load can be modeled by a large laser head inductance in series with a small time-varying discharge resistance. The 30 nsec collapse of the discharge resistance and the large head inductance lead to impedance mismatch and large voltage reflections. These reflections can reduce the overall efficiency of the laser. However, SRL has developed energy recovery circuits which recover a large fraction of the pulse energy reflected from the discharge. This energy is returned to the primary energy storage capacitors and then reused on the next pulse. With these circuits, the electrical coupling efficiency to copper vapor laser loads has been increased by 50% over that achieved with thyratron-based drivers.

III. WORK PLAN

In this section we will present a detailed strategy used to develop an all-solid-state driver for a high power, excimer laser optimized for the P-GILD process. We begin with a summary of the research results obtained from a breadboard driver that was designed, fabricated, and tested on a high power, excimer laser head at Cymer, Inc. We will continue with a description of how these results were applied to the development of a full production prototype.

The laser parameters were chosen to provide the best compromise to the demands of a wide variety of applications for ablative laser technology. For the high power laser development program, we opted to maintain the same gas chemistry, KrF/Ne at 248 nm, Cymer presently utilizes for low power lithography. The final choice of the optimum wavelength for P-GILD is also unknown at this point. A change is gas chemistry have necessitated the construction of a separate laser final assembly facility in order to prevent contamination.

In spite of the fact that the Cymer high power laser development program is presently centered around 248 nm, the single pulse energy and repetition rate goals are almost identical to those presently envisioned for P-GILD. This driver development program affords a valuable opportunity for SRL and for Cymer. We demonstrated through early experiments that a thyratron-based pulsed power system will never be able to deliver the cost of ownership demanded by the marketplace. All-solid-state drivers with their almost infinite lifetime and invaluable energy management capabilities reduce electrode wear and extend chamber life in addition to eliminating the cost of thyratron replacement. The culmination of this joint research project was a high power excimer laser well suited to a wide variety of applications including, but not limited to, P-GILD.

IV. Experimental Results

In the past, Science Research Laboratory has worked with Cymer, Inc. on the development of advanced, line narrowed excimer lasers for application to DUV lithography. The program was highly successful providing a demonstration of the effectiveness of all-solid-state driver technology in improving performance and reducing cost of ownership of excimer lasers. These DUV lithography lasers while providing a useful example are not sufficiently powerful to be directly useful in the P-GILD process. The P-GILD process, sometimes called "ablative lithography" requires lasers that deliver average output powers approaching 200 watts as opposed to the 10 watts required for more conventional lithography.

We began our research program by engaging in extensive discussions with representative of both the end users at Ultratech and Cymer, Inc. This program presented some unique opportunities and challenges. Unlike the previous joint effort with Cymer involving line-narrowed, DUV lithography lasers where the laser already existed albeit with a thyratron-based pulsed power driver, in this project a final version of the P-GILD laser did not exist at Cymer. The development project for both the laser and modulator would have to be conducted in parallel.

Cymer eagerly agreed to help support the modulator development project providing additional financial support. This allowed us to fabricate a complete breadboard modulator and demonstrate its effectiveness. The design parameters for this breadboard laser driver are listed below.

Table I - Laser Driver Requirements

Average Output Power	$\leq$ 8 kilowatts
Single Pulse Output Energy	$\leq$ 20 Joules
Peak Voltage	$\leq$ 25 kilovolts
Pulse Risetime (10% to 90%)	150nsec(C_{peak}=60nfd)
Pulse Repetition Rate	$\leq$ 300Hz initially (400 Hz final)
Laser Output	$\geq$ 300pps X 0.50 J/pulse (150 watts)

This research effort culminated in the construction of the XLD-IV (Excimer Laser Driver - IV), a breadboard, all-solid-state, nonlinear pulsed modulator. It consists of:

1) a Commutator Module housed in a 16" high, rack mountable unit pictured in Figure 2.;

2) a Compression Head which serves as the Laser Interface Module pictured in Figure 3.

XLD-IV was fabricated to serve as the backbone for the effort and was delivered to Cymer. XLD-IV was constructed to collect data on the laser-driver interface requirements. The final experimental results from the tests with XLD-IV provided the necessary data to design and fabricate a production prototype complete with all of the features deemed appropriate for the P-GILD mission. This production prototype, all-solid-state driver was fabricated, delivered to Cymer and tested on an excimer laser head.

The XLD-IV driver is a 0-10 kilowatt output, 80% efficient, all-solid-state discharge power source. A simplified schematic of XLD-IV is presented in Fig. 4, while the performance specifications of XLD-IV are listed in Table II.

The $\leq$ 30 Joules stored in the 61μF intermediate storage capacitor is transferred to the 1st stage of the compression network during a 25 μsec commutation cycle. The compression circuits take this energy and temporally compress it into a 120 nanosecond pulse at the end of the chain. The voltage is also increased from the input voltage level of 1 kV to the output voltage level of 28 kV. This entire process is completed with a measured efficiency of over 80%. XLD-IV incorporated energy recovery circuits which store the reflected energy from the laser head and add it to the energy in the next pulse, thereby increasing laser efficiency and reducing electrode erosion.

In Fig. 5, Cymer has supplied a measurement of the voltages appearing on each stage of the XLD-IV driver during a compression cycle. The time scales vary from 200 nanoseconds per division in the uppermost scale where the final laser voltage appears, to 50 microseconds per division in the lowermost scale where the SCR commutator output is presented. The overall temporal compression factor of the XLD-IV driver reaches $\simeq$200:1. The peak output power level exceeds 200 megawatts.

Measurements of the laser voltage waveshape, discharge current, fluorescence and lasing intensity are presented in Figure 6. A plot of laser energy output versus power supply voltage at 250 Hz and 10 Hz shown in Fig. 7 indicates a maximum laser power output of $\simeq$140 watts. The plot presented in Fig. 8 shows that the overall driver efficiency is 80%. In order to qualify these results, it is important to note that the results plotted in Fig. 7 represent operation with a new set of electrodes and a new laser gas mix. Over the lifetime of a laser chamber, the output degrades and output power levels on the order of 100 watts are more typical of a chamber at end of life. In order to provide a reliable 200 watt output over the entire laser maintenance cycle, we increased the output power approximately two-fold over our present results.

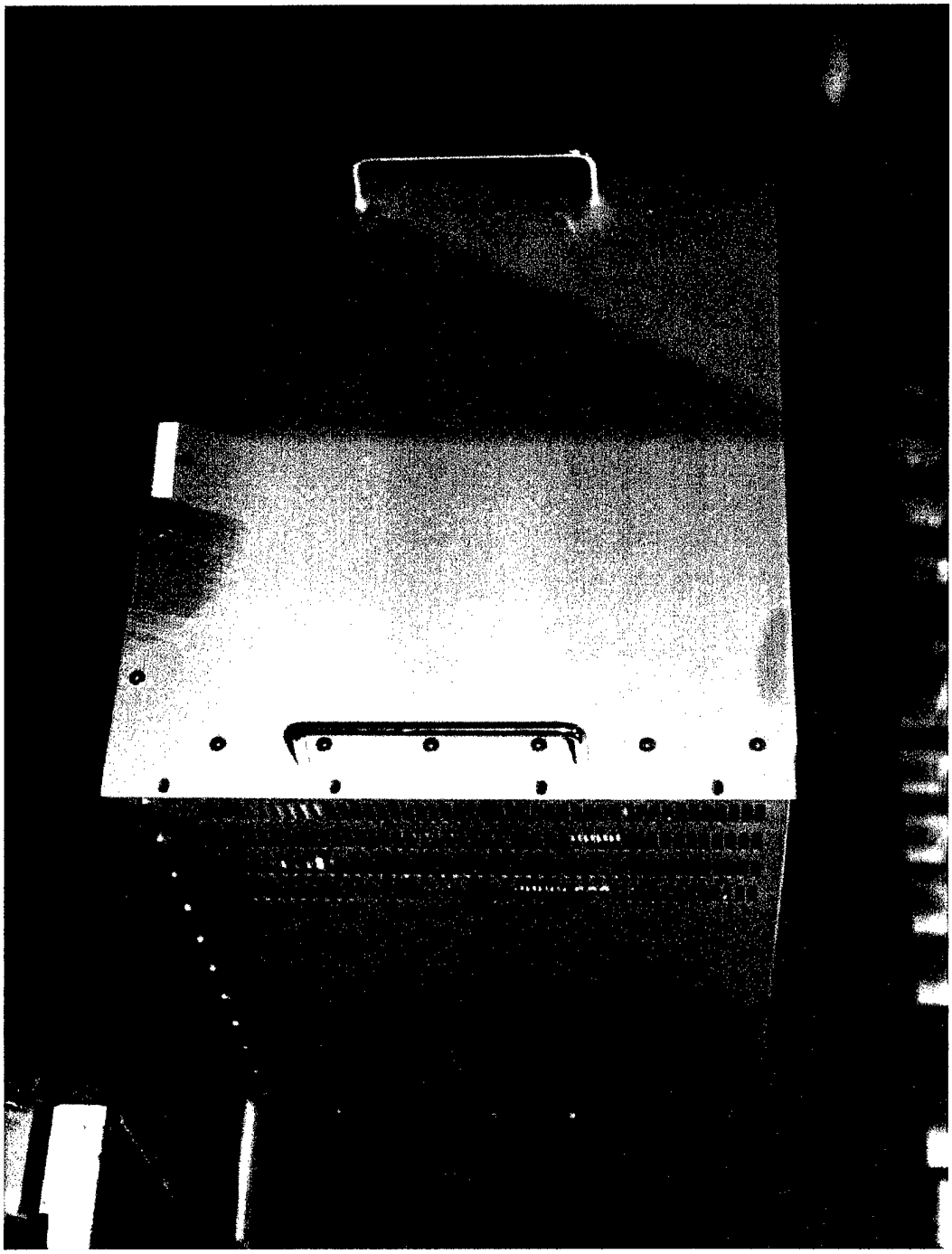

Figure 2: XLD-IV Commutator Module

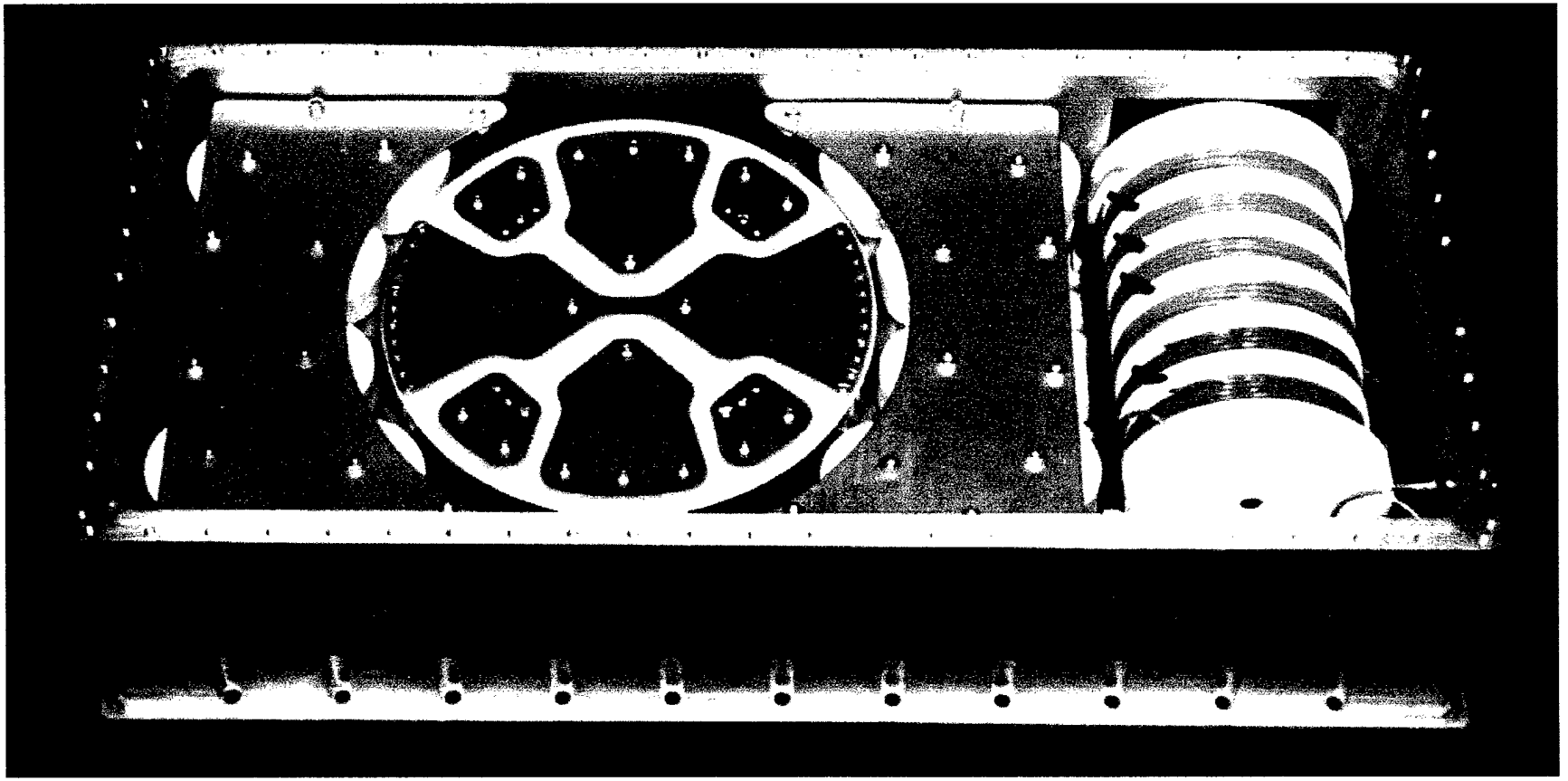

Figure 3: XLD-IV Compression Module

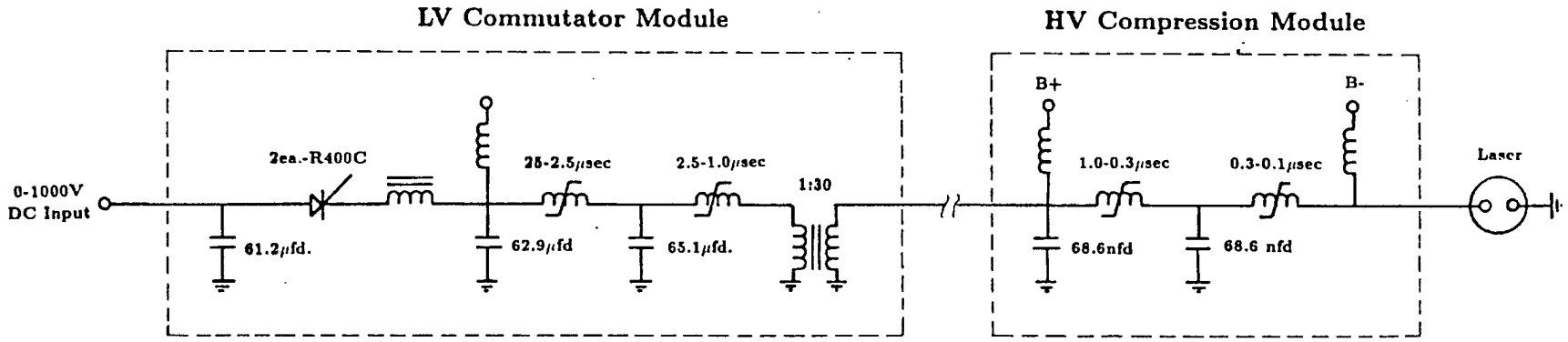

Figure 4: XLD-IV Simplified Schematic

Table II: XLD-IV Performance Specifications

Input Power Requirements:	
Energy/pulse	$\leq$30.58 joules
PRF	$\leq$1 kHz
Power	$\leq$30.58 KW
Voltage	$\leq$1000 volt
Current	$\leq$30.58 Amps
Intermediate Storage	
Capacitance	61.16 μfd
Voltage	$\leq$1000 volts
Energy	$\leq$30.58 joules
Stored charge	$\leq 61.16 \times 10^{-3}$ Coulombs
τ discharge	$\leq$25 μsec
I peak	3.84×10^{3} Amp
dI/dt	0.483×10^{3} A/μsec
dI/dt per device	242 A/μsec
Commutation losses	$\sim$ 0.5 joules
1st Stage	
Capacitance	62.92 μfd
Voltage	$\leq$978 volts
Energy	$\leq$30.08 joules
Core Type	0.6 Mil x 2605 SC
Core Dim.	9.6"OD X 2.5"ID X 2.0"Wide
$\int V \cdot dt$	$\sim 12 \times 10^{-3}$ Vsecs
Lsat	15 nh + 5.4 nh (STRAY) = 20.4 nh
τ discharge	2500 nsecs
Losses	$\sim$ 0.9 joules (0.5 cores, 0.4 caps)
Core volume	1.55×10^{-3} m^3, 10.83 kg
2nd Stage	
Capacitance	65.12 μfd
Voltage	$\leq$947 volts
Energy	$\leq$29.18 joules
Core Type	0.6 Mil x 2605 SC
Core Dim.	9.6"OD X 8.0"ID X 2.0"Wide
$\int V \cdot dt$	$\sim 1.44 \times 10^{-3}$ Vsecs
Lsat	2.0 nh + 1.26 nh (STRAY) = 3.26 nh
τ discharge	1000 nsecs
Losses	$\sim$ 1.2 joules (0.5 cores, 0.7 caps)
Core volume	$.435 \times 10^{-3}$ m^3, 3.044 kg
Transformer	
Core Type	2605S3A
# Turns (PRIM)	1/30
# Turns (sec)	1
Losses	$\leq$ 1.0 joules
Peak stress	26 kV/cm at 30 kV
Core geometry	30 x 0.875" ID x 1.75" OD x 1.0" wide
3rd Stage	
Capacitance	68.56 nfd
Voltage	$\leq$28 kV
Energy	$\leq$27 joules
Core Type	3t X 50-50 Ni-Fe
Core Dim.	6.25"OD X 3.5"ID X 2.0"Wide

Table II: XLD-IV Performance Specifications (Continued)

$\int V \cdot dt$	$\sim 14 \times 10^{-3}$ Vsecs
Lsat	62.6 nh + 25 nh (STRAY) = 87.6 nh
τ discharge	172 nsecs
Losses	$\sim$ 1.0 joules (0.6 cores, 0.4 caps)
Core volume	$.587 \times 10^{-3}$ m^3, 4.69 kg

4th Stage

Capacitance	68.56 nfd
Voltage	$\leq$27.5 kV
Energy	$\leq$26 joules
Core Type	3t X CN-20 Ferrite
Core Dim.	8.0"OD X 4.0"ID X 1.0"Wide
$\int V \cdot dt$	$\sim 2.5 \times 10^{-3}$ Vsecs
Lsat	35 nh + 15 nh (STRAY) = 50 nh
τ discharge	122 nsecs
Losses	$\sim$ 1.2 joules (0.5 cores, 0.7 caps)
Core volume	$.617 \times 10^{-3}$ m^3, 3.1 kg

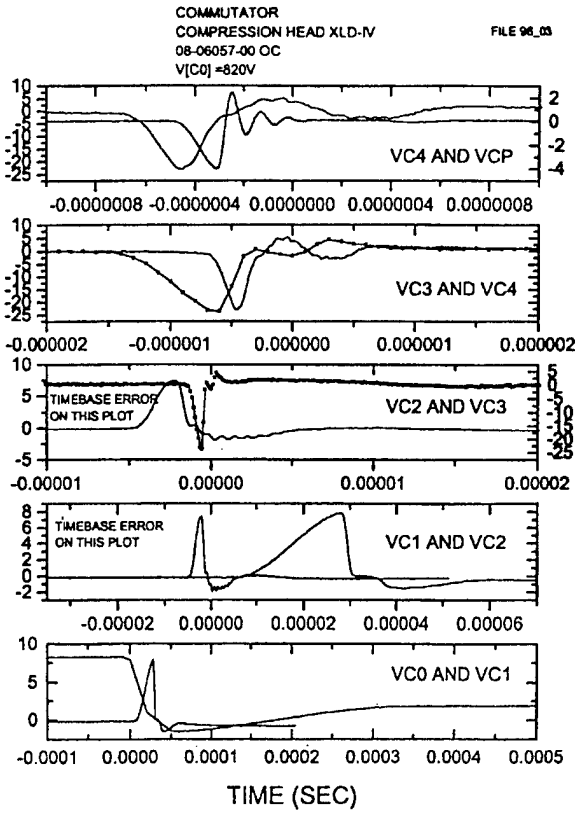

Figure 5

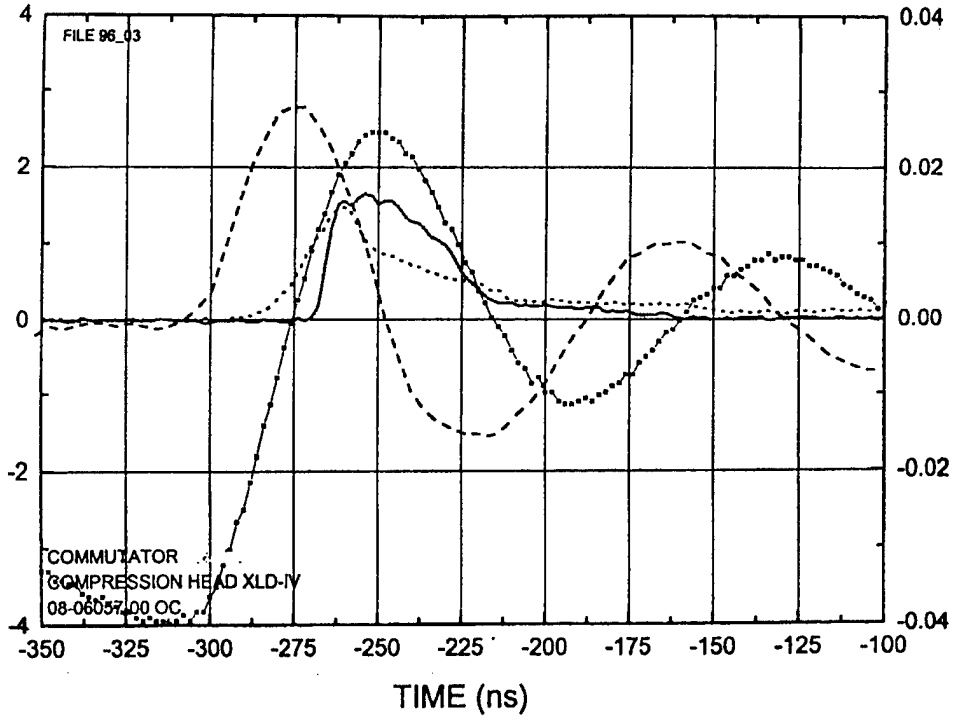

Figure 6: V[CP], Discharge Current, Fluoresence and Lasing at 820 V

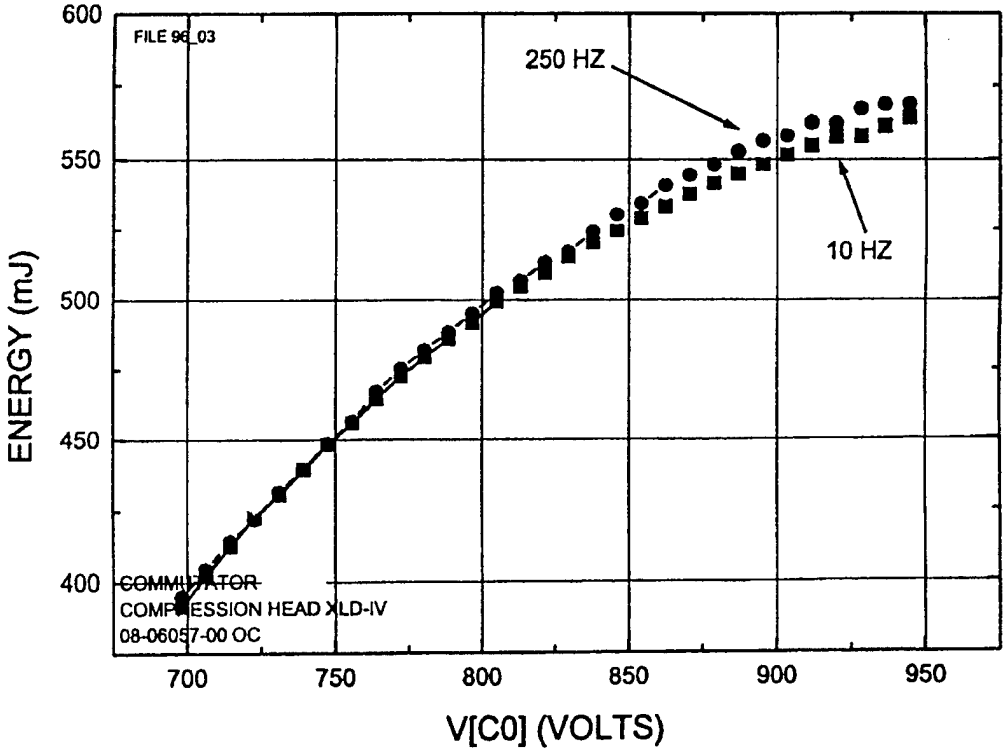

Figure 7: Measured DE/DV

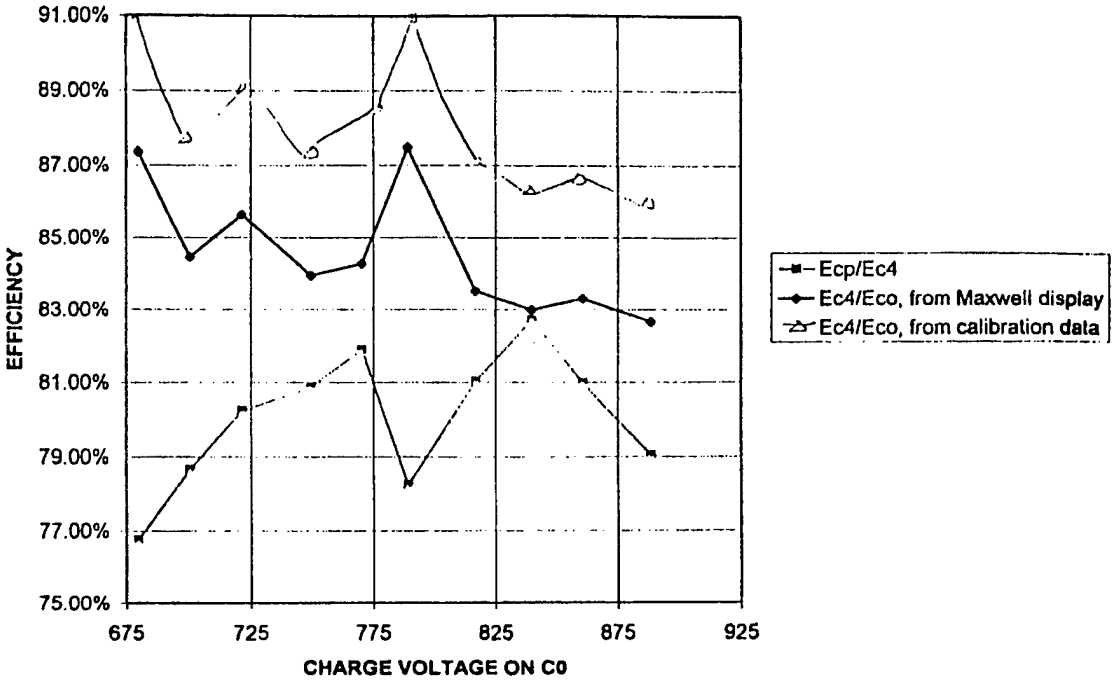

Figure 8: SSPPM Transfer Efficiencies

We continue with a brief description of the operating principle behind the XLD-IV, all-solid-state driver and follow that section with a more detailed description of the complete XLD-IV driver system.

Nonlinear Magnetic Compressors

The XLD-IV driver utilizes commercially available Silicon Controlled Rectifiers (SCRs) as initial commutators. These devices transfer the energy stored in a primary capacitor bank into the pulse compression chain. While this transfer time (typically 25μsec at a peak power of ~1 Megawatt) has been selected to keep the commutators well within specifications, it is far from the 200-300 Megawatt output peak power required by the laser load. The technique of providing power multiplication via temporal compression of the stored energy is a primary design innovation developed for this modulator. The energy transfer time is reduced while the energy remains constant resulting in power amplification. This useful concept is accomplished through careful utilization of the properties of nonlinear magnetic material.

The concept of using saturable reactors to construct high power pulse generators is not a new concept and certainly not invented by the authors, but there have been few recent applications of this technology. The use of saturable reactors for high power pulse generation was first described by Melville in 1951. At that time, output powers levels as high as a megawatt were being sought for radar applications. There were no SCRs at the time and thyratrons were rapidly developed to the point where they could deliver these power levels routinely and the idea of nonlinear magnetic pulse compression simply disappeared. The development of induction

linear accelerators and discharge lasers requiring gigawatts of input power revived this old technology.

The basic principle underlying nonlinear magnetic driver operation involves using a saturable core as an inductor in a resonant circuit. The circuit is designed to allow the core of the next stage to saturate before a significant fraction of the energy stored in the capacitors of the previous stage is transferred. This nonlinear saturation phenomenon shifts the resonant frequency of this resonant circuit by the square root of the permeability shift as the core saturates. These stages are typically cascaded (Fig. 9) and energy is coupled faster and faster from one stage to the next. These circuits are efficient at transferring power in both directions since they act not only to upshift the frequency in the forward direction thereby providing temporal compression, but also downshift the frequency of a voltage pulse as it cascades back up the chain in the reverse direction. The energy that reflects from the mismatched load can be saved and applied to the next pulse.

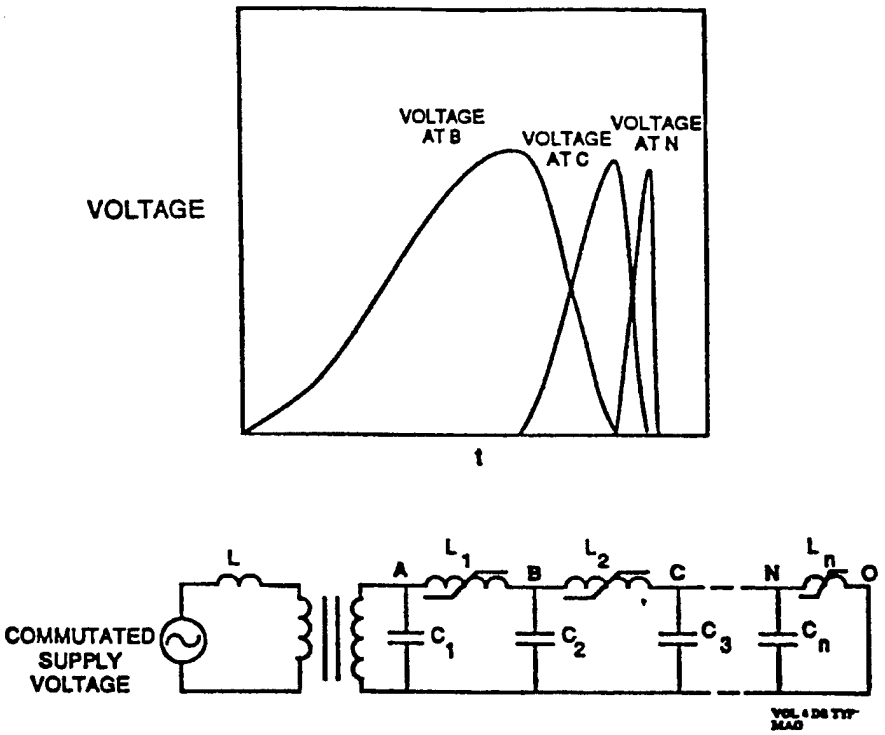

Figure 9: Typical magnetic switch operation

In the remainder of the section we present a more quantitative description of the compression chain operation. The analysis is based on saturable inductors with toroidal geometries, and for the sake of clarity several simplifying approximations have been introduced. All circuit components will be assumed lossless and all extraneous inductances ignored. Also the expression for saturated inductance will assume that the area enclosed by the turns is simply the core cross-sectional area, while in practice the packing factor must be properly calculated.

Saturation of an inductor occurs when the magnetic field in the inductor core reaches the saturation magnetization. This assumes of course that the core material is ferri- or ferromagnetic material. Saturation is measurable as a large incremental change in the material permeability.

According to Maxwell,

$$\int E \bullet dl = V_L = N\frac{\partial \phi}{\partial t} = NA\frac{\partial B}{\partial t}$$

$$\int V_L dt = NA\Delta B$$

and if the core has been reset

$$\int_0^{\tau_{sat}} V_L dt = NA(-(-B_r) + B_s) = NA\Delta B_s$$

where N is the number of turns around the core, A is the area of the core, and B_r (B_s) the remanent (saturating) magnetic field.

If we make all of the capacitance values in the compression chain equal to C_0, then for a capacitor preceded in the chain by L_{n-1} and followed by L_n the time required to charge the next capacitor in line after inductor L_{n-1} saturates is given by

$$\tau_{charge}^{C_n} = \tau_{discharge}^{C_{n-1}} = \pi\left(L_{n-1}^{sat} \cdot \frac{C_{n-1}C_n}{C_{n-1}+C_n}\right)^{1/2} = \pi\left(\frac{L_{n-1}^{sat} \cdot C_0}{2}\right)^{1/2}$$

The time required to charge capacitor C_n should be designed to be approximately equal to the time to reach B_{sat} in inductor L_n. Therefore

$$\tau_{sat}^{L_n} \approx \tau_{charge}^{C_n} = \frac{\Delta B_s N_n A_n}{\overline{V_c}}$$

Ideally

$$\overline{V_c} = V_{C_0}\int_0^{\pi/\omega} \frac{(1-\cos\omega\tau)}{2} dt = \frac{V_{C_0}}{2}$$

therefore

$$\tau_{charge}^{C_n} \approx \frac{2\Delta B_s}{V_{C_0}} N_n A_n$$

where V_{C_0} is the peak charge voltage of capacitor C_n. After inductor L_n saturates we find:

$$L_n = \frac{\mu_n^{sat}}{2} w_n N_n^2 \ln\left(\frac{R_{0_n}}{R_{i_n}}\right) \approx \frac{\mu_n^{sat} N_n^2 A_n}{2\pi\overline{R}} \approx \frac{\mu_n^{sat} N_n^2 A_n}{\text{volume}}$$

where w_n is the axial width of the toroid $R_{0_n}(R_{i_n})$ the core outer (inner) radius. It also follows that if the core saturates at the peak of the charging waveform then

$$L_{n-1}^{sat} = \frac{2}{C_0}\left(\frac{2\Delta B_s N_n A_n}{\pi^2 V_c}\right)^2$$

and

$$\frac{L_n^{sat}}{L_{n-1}^{sat}} \approx \frac{\mu_n^{sat}\pi^2}{\text{volume}_n} \cdot \frac{(\frac{C_0}{2}V_c^2)}{4\Delta B_s^2} \approx \frac{\text{energy}}{\text{volume}_n}\left(\frac{\mu_n^{sat}\pi^2}{4\Delta B_s^2}\right)$$

since

$$\text{gain} = \frac{\tau_{charge}^{C_n}}{\tau_{charge}^{C_{n+1}}} = \left(\frac{L_n^{sat}}{L_{n+1}^{sat}}\right)^{1/2}$$

The core volume requirement to produce a given temporal compression and corresponding energy gain is given by

$$\text{volume}_n = \text{gain}^2 \text{energy}\ \left(\frac{\mu_n^{sat}\pi^2}{4\Delta B_s^2}\right)$$

In practice not all of the fields are confined to the core and if we define the packing factor pf to be the ratio of the inductance calculated by assuming all of the magnetic field energy is stored in an ideal saturated toroid to the actual measured saturated inductance, then our core volume requirement can be rewritten as

$$\text{volume} = \text{gain}^2 \cdot \text{Pulse Energy} \cdot \left(\frac{\mu_o \cdot \pi^2}{4 \cdot (\Delta B_s \cdot \text{pf})^2}\right)$$

The packing factor is defined as

$$pf = \frac{\int_{V_f} H^2 dv}{\int_{all\ space} H^2 dv}$$

where V_f is the actual volume occupied by the ferri- (ferro) magnetic core material excluding all interlaminar insulation and voids. Optimization of this packing factor is crucial in magnetic switch design and is accomplished by enclosing the core in a tightly fitting conducting housing. The multiple turns are formed as coaxial transmission lines which pass through this housing. Circulating currents set up in this housing exclude the magnetic flux and contain it in the desired volumes.

With the saturable material completely enclosed in conducting coaxial housings, the voltage per turn associated with the dB/dt of the core appears across a single narrow gap on the outside diameter of each housing. Connecting the coaxial transmission lines in the inner and

outer housings with radial transmission lines across the top and bottom of the core completes the turns. The impedances of these transmission lines are adjusted so that

$$Z_{LINE} \approx \sqrt{\frac{2 \cdot L_{sat}}{C}}$$

while simultaneously every effort is made to minimize $L_{sat} \bullet C$ which is proportional to the square of the pulse length. Here L_{sat} and C refer to the saturated inductance of the reactor and the value of the storage capacitance respectively.

The XLD-IV Commutator Module

The 16" high rackmountable Commutator Module includes commutators, initial compression stages, 1:30 induction-style step-up transformer, control circuitry, and bias supplies. All required trigger amplifiers along with housekeeping and protection electronics are enclosed within this module. With the exception of a 1000 Volt capacitor charging supply, the Commutator Module requires only a TTL trigger input and 24 VDC. The 24 VDC input runs all of the interior ancillary electronics. The ancillary electronics are all housed within the Control Electronics Bay at the bottom of the Commutator Module and are fully shielded from the high power electronics. The highest voltage appearing in this bay is 24 VDC.

The control electronics monitor driver operation and terminate normal operation if it senses a problem. One very key component incorporated within the Commutator Module is the Energy Recovery circuitry. This circuit recovers any energy reflected from the load and adds this reflected energy to the forward energy in the next pulse. The control electronics carefully monitor the level of recovered energy and sense any irregularity. If the level of recovered energy exceeds a preset level with respect to the forward energy, the modulator will ignore trigger pulses for a period of 0.1 seconds, assuming that there may be an arc at the output. The 0.1 second delay will allow for recovery of an electrical breakdown, but if the mismatch persists the modulator will be limited to 10 Hz operation. The control electronics also limit peak operating voltage, PRF, and input current to the modulator.

The HV Electronics Bay of the Commutator Module contains the initial energy storage capacitors (C_0), commutators, charge inductor, first stage energy storage capacitors (C_1), 1st stage saturable reactor, second stage energy storage capacitors (C_2), 2nd stage saturable reactor, and 1:30 induction-style step-up transformer. The capacitors are low loss, high reliability, polypropylene, commutator capacitors. The commutators can be chosen either to be fast recovery, inverter Silicon Controlled Rectifiers (SCRs) or Insulated Gate Bipolar Transistors (IGBTs). The charge inductor is constructed from high frequency litz wire and is designed to limit the peak current and dI/dt to well within the ratings of the SCRs and/or IGBTs. In the case of XLD-IV, the energy transfer time from C0 to C1 determined by this inductor has been chosen to be approximately 25μsec.

With an energy transfer time of 25μsec from C0 (61μfd, 0-1000V, 0-30 Joules), the initial energy storage capacitor, to C1 (63μfd, 0-978V, 0-30 Joules), the first stage energy storage capacitor, the peak power handled by the commutators is only around a megawatt.

The Commutator Module utilizes two stages of compression to reduce the 25 μsec energy transfer time provided by the commutators to the 1.0 μsec energy transfer delivered to the primary of the 1:30 induction-style, step-up transformer. The peak power is multiplied by a factor of 30 through these initial compression stages while 93% of the energy is conserved.

The 1:30 induction-style transformer converts the 0-1000 Volt operation of the Commutator Module to the 0-28 kilovolt requirement of the load. The 0-1000 Volt operating level used within the Commutator Module was selected to eliminate corona and breakdown problems associated with higher voltages and facilitate the choice of commutators and capacitors. Up to the input of the transformer, we have not been required to utilize voltages in the tens of kilovolts and through the use of a unique transformer design, we can avoid that problem even at the transformer. A short section of HV cable replaces the charged particle beam in this accelerator. The voltage appears inside the cable on the center conductor but nowhere else in the chassis. Even at the high voltage output of the transformer, exposure to high voltage is avoided.

The high voltage charging pulse, 1.0 μsec in duration with a peak voltage of 0-28 kilovolts and peak power of 0-30 Megawatts, exits the Commutator Module through a length of double shielded RG-177 coaxial cable which connects to the HV Compression Head.

The XLD-IV Compression Head

The smaller, sealed, High Voltage Compression Head (Figs. 10 and 11) serves primarily as a laser interface. Interior components can be changed at will to provide various risetimes and per pulse drive energy to the gas discharge load. It has initially been loaded with a two stages of compression that reduce the energy transfer time from 1.0 μsec to 122 nanoseconds. The actual peak output voltage and risetime at the load will depend on the choice of peaking capacitor. At a maximum peaking capacitor load of 60 nfd, the peak output voltage is 27 kV.

V. FLOW TECHNOLOGY DEVELOPMENT FOR HIGH POWER, HIGH REPETITION DUV LASERS

SRL has developed the gas flow technology for a high repetition rate excimer lasers. The industry uses excimer lasers that radiate at a wavelength of 248 nm and operate at a pulse repetition rate of 700 pps. Much effort has been spent in attempts to increase the pulse repetition rate of excimer lasers by making systematic modifications to an existing Cymer laser head configuration. The objective of this effort has been to achieve a dramatic increase in pulse repetition rate of these lasers, primarily through changes in the laser gas flow subsystem.

Major elements in any gas laser recirculating subsystem (flow loop) include the discharge cavity, recirculating fan, heat exchanger for removal of both discharge and fan deposited power, and acoustic suppression to attenuate pressure waves which result from pulsed gas heating.

Gas which is heated by the pulsed discharge must be swept clear of the cavity prior to the subsequent laser pulse. This is necessary to provide a homogeneous cavity gas medium and for the prevention of arcing during the discharge. The required volume of gas flushed through the cavity between pulses is determined experimentally and is based on current experience at Cymer. This normalized clearing volume, defined as the flush factor, combines with the cavity volume

and laser pulse rate to provide a fan flow rate requirement. Pressure loss around the gas circulation loop is determined both by element flow analyses and mock-up flow tests to provide a fan pressure rise requirement. These two fan requirements are the basis for selection of both fan class and size.

Program Approach

The goal of the program had been to achieve a fivefold increase in laser pulse rate (from 700 pps to 3,500 pps) by a reduction in the cavity cross section in proportion to the increased pulse rate at fixed average power. Pulse energy would be reduced by maintaining fixed average laser power while increasing pulse rate. This reduction in cross section was to be achieved by a 2.5X reduction in cavity discharge heigh and a 2.0X reduction in cavity discharge length (in the flow direction). These reductions would have resulted in a 2.5X increase in cavity flow speed at fixed volumetric gas flow rate. This approach is shown in figure 12.

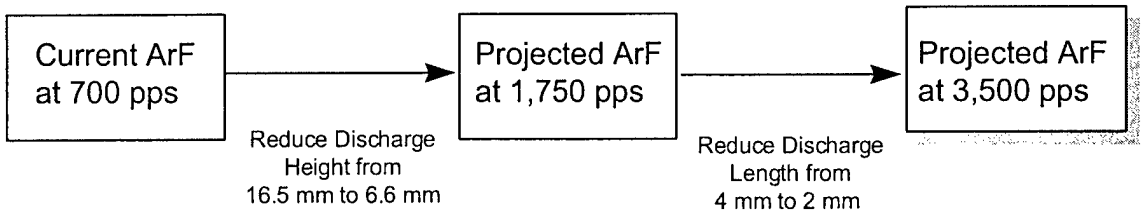

Figure12. Discharge Cavity Scaling Rationale

1. Develop a scaling rationale for a fivefold increase in laser pulse rate.
2. Employ the existing Cymer fan motors, drives and couplings with a nominal unit power capability of 1.0 SHP, or make design modifications on the basis of their design, as required, for higher power demand
3. Use most recent excimer laser performance, as demonstrated at Cymer, as the basis for performance scaling.
4. Model Fan performance characteristics as follows:
    - Apply established fan scaling relations to project flow requirements for 3,500 pps laser operation
    - Use LAU fan performance specifications curves to identify operating regimes in terms of degree of stall and fan efficiency. The LAU fan performance specifications would be supplemented with experimental data using an open-loop ducted flow facility
    - Apply specifications and scaling to the current Cymer laser head configuration.
    - Apply specifications and scaling to a configuration with a fan of reduced length in relation to the discharge length.

5. Scale flow performance to estimate the maximum practical excimer pulse rate which is achievable with the existing Cymer flow configuration. Verify this with flow measurements at SRL using the Cymer ELS Flow Model with modifications.
6. Develop a brassboard flow subsystem concept design on the basis of the results and conclusions from the above studies that would interface with the Cymer discharge design for a 3,500 pps laser demonstration.
    - Build and test model of this brassboard flow subsystem to verify projected flow performance.
    - Incorporate and test potential improvements in this flow model throughout the course of the research and development
    - Build, assemble and test the Brassboard System for a 3,500 pps excimer laser demonstration.

Baseline Cavity Discharge Scaling Rationale

The original program approach was modified as a result of Cymer's testing and development of the laser system, Cymer's test results showed arc-free laser performance was not achievable with a *2.5X* reduction in cavity discharge height. Therefore, the baseline laser head configuration was re-defmed to match Cyiner's ELS discharge height of 16.5 mm, instead of the 2.5X reduction to 6.7 mm. The general consensus was that the best excimer laser performance demonstrated at Cymer, 2200 pps with a cavity flow speed of 28 m/sec, would be used as the basis for performance scaling to 3,500 pps instead of Cymer's rated performance at 700 pps. This has the effect of scaling volumetric flow as well as cavity velocity with pulse rate.

Table 3 summarizes the resulting effect of adapting this baseline approach to the Brassboard Laser flow requirements. The Brassboard Laser flow performance requirements, based on the original program approach are listed in the second column in Table 3. These requirements had been scaled from Cymer's excimer laser operation at 700 pps with their ELS laser series as listed in the first column in Table 3. The baseline Brassboard design requirements are listed in the fourth column in table 3. These requirements have been scaled from Cymer's best excimer operation at 2,200 pps as listed in the third column in Table 3. A comparison of the original and baseline flow performance requirements shows the baseline approach, shown in Figure 13, has the affect of 1) increasing the deposited electrical power, 2) increasing fan power demand since volumetric flow is now scaled with pulse rate, and thereby 3) increasing heat exchanger loading.

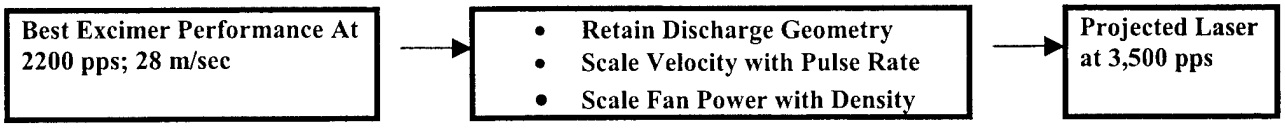

Figure 13. Baseline Discharge Cavity Scaling Rationale

Table 3. Brassboard Design Requirements

	Cymer's ELS Configuration Excimer Operation	Scaled Brassboard (Original)	Cymer's Best Excimer Performance	Scaled Brassboard (Baseline)
Pulse Rate (pps)	700	3,500	2,200	3,500
Fan Speed (RPM)	2,500	5,000	3,800	4,400
Discharge Height (mm)	16.5	6.7	16.5	16.5
Discharge Width (mm)	4.0	2.0	4.0	4.02
Pressure (Atmospheres)	4.5	4.5	3.6	3.6
Temperature (°C)	55.0	55.0	55.0	55.0
Laser Gas Density (kg/m^3)	3.37	3.37	2.70	2.70
Gas/Air Density Ratio (σ)	2.85	2.85	2.28	2.28
Flow Speed (m/sec)	17	42.5	28.0	42.5
Fan Power Demand (W)	570	1,950	700	1,890
Deposited Electrical Power (W)	3,400	3,400	5,500	10,500

VI. DEVELOPMENT OF THE FLOW SUBSYSTEM

The flow loop configuration and overall size is, to a large extent, dictated by the selection of fan type. For a specified gas flow rate, options of tangential (or cross-flow) fans, vane-axial fans and centrifugal fans are typically selected in that order for increasing pressure rise requirements. For closed loop laser applications, an addition driving consideration is system compactness and simplicity in configuration. Fans in these three classes require increased configuration complexity and size in the order listed above.

Tangential fans provide an excellent match to laser geometries. Tangential fans lave a large ratio of length to diameter and propel the gas in a two-dimensional manner through a turn. This provides an excellent match to laser applications that require uniform flow across a small optical aperture transverse to a long optical axis. Due to the resulting compact flow loop, this is the fan of choice for most commercial lasers.

Performance Features of Tangential Fans

Extensive fan performance tests have been conducted utilizing SRL's Open loop and Closed Loop Flow facilities, as shown in Figure 14 and Figure 15. These tests have served to: 1) establish the flow regimes in relation to stall; 2) establish the database for scaling of manufacturer's performance specifications; 3) establish the effect of changes in fan geometry on performance; and, 4) provide an intermediate tool for the development of the Brassboard Flow System.

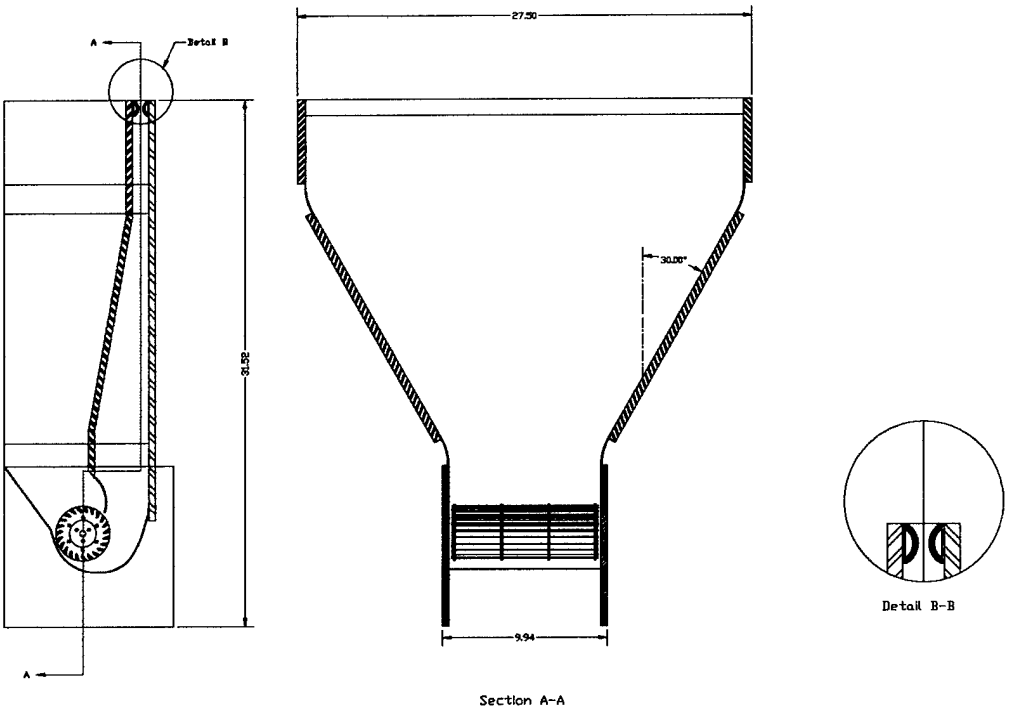

0232-028

Figure 14. SRL's Open Loop flow Facility: Tangential Φ3.26" x 8.25 Fan

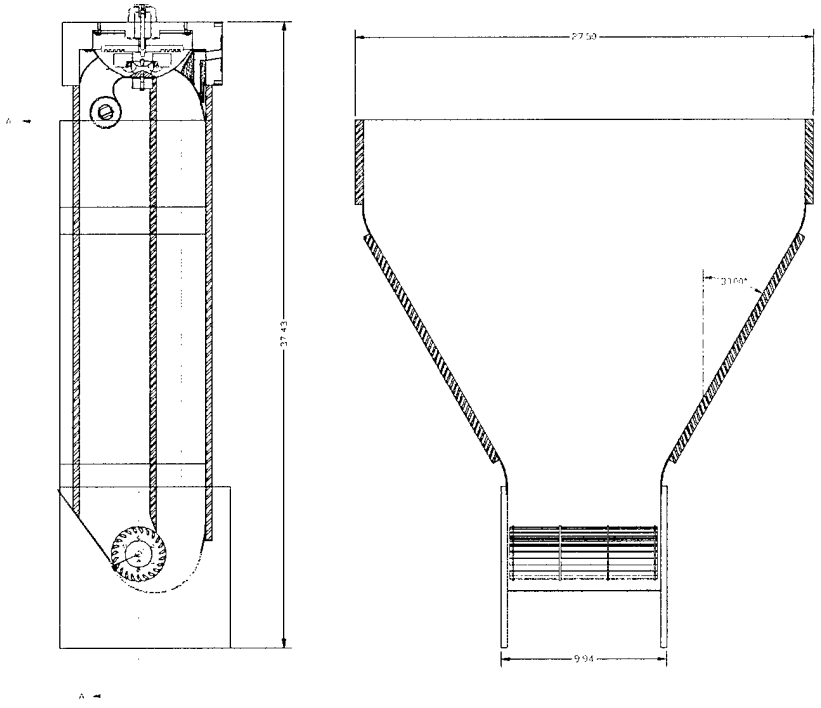

Figure 15. SRL's Closed T#-8.25 Flow Test Facility

These test results show that scaling to high laser pulse rates is most easily achieved by utilizing a tangential fan whose length is optimized or tuned for a particular cavity discharge height. For the original 2.5X reduction in cavity discharge height (6.7 mm) the desired nominal fan length is 9" whereas for the baseline cavity discharge height of 16.5 mm the nominal fan length is 17". Since the optimal fan length is shorter than the laser discharge length (along the optical axis), higher rotational speeds are allowed by increasing the critical speed and fan operation is shifted well away from the stall regime.

Utilizing the shorter fan lengths does require a transition section between the fan and the cavity to disperse the flow to uniformly fill the cavity over the discharge length. Turning vanes would not be required in the transition section because test results have shown that the fan serves effectively as a static pressure source. This allows a very simple transition geometry between fan and cavity since turning vanes are unimportant when flow dynamic pressure is small in comparison to the total pressure. These transitions dictate a modest increase in flow loop volume.

Conclusions from SRL's Open loop and Closed Loop Flow facilities test results include:

- Cavity flow speed varies linearly with fan speed.
- A shortened fan is well tuned to reduced discharge height (6.7 - 10 mm).
- No stall occurs over the entire length of the fan.
- A shortened fan provides higher cavity flow velocity at any given fan speed.
- Good cavity flow uniformity is achieved with a simple (no vanes) and short fan to cavity transition section.
- Demonstration of (original) required performance provided the rationale for SRL Brassboard Flow System design.
- Test results also provided guidance in flow system design to meet baseline operational requirements.

Brassboard Flow Subsystem Configuration

The SRL flow subsystem was selected as baseline on the basis that the design offers many advantages over the current Cymer ELS configuration. These include: 1) ample, nonintrusive space to accommodate the fan motors; 2) flexibility for design modifications with a bolt-on fan box; 3) ample space to accommodate the heat exchangers for increased heat rejection requirements; 4) added margin in fan speed and flow capability; and 5) compact design to integrate easily in the current available space of a representative excimer laser system. The SRL design incorporates two fan motors of current Cymer design which fit in recesses under the discharge head so that there is maximum access for integration of optical components to the laser. This design also allows implementation of the Cymer technology in areas of motor control, presssure/vacuum interfaces and seals, and bearing configuration and supports. The interface plane between the two subsystems is shown in Figure 16. Section views of the flow subsystem, integrated with a representative Cymer discharge design are shown in Figure 17 and Figure 18

The brassboard flow subsystem was originally configured with two finned heat exchanger tubes for a total heat rejection capability of 5,600 W along with a nominal 9-inch long tangential fan. Due to the increased heat loading and flow requirements of the baseline

configuration, the SRL Brassboard Flow Subsystem design was modified to accept 1) four finned heat exchanger tubes for a total heat rejection capability of 12,400 W and 2) a nominal 17-inch long tangential fan.

Acoustic suppression is achieved by addition of perforations in various inner flow walls. These perforations typically have an open area fraction of a few percent and consequently do not alter current flow system performance

Heat Exchanger Subsystem Design

The heat exchanger design is a complex process not only because of the variety of heat exchanger configurations and parameters available but also because of conflicting requirements for closed loop laser applications. The heat exchanger size has to be as small as possible to 1) limit loop pressure drop thereby reducing fan power requirements, and 2) maintain flow loop compactness. However, it needs to be large enough to adequately meet the heat load requirements. Material choices and fabrication procedures are another constraint to prevent laser gas contamination or depletion. SRL's existing fm/tube heat exchanger computer code was modified to facilitate the design of the brassboard heat exchanger. The design approach and data given by Kays and London[1] was used as a guide for the heat exchanger code and analysis.

The heat exchanger configuration chosen, as shown in Figure 18, consists of finned tubes with a fin OD of 1.00", and tube OD of 0.50". The tubes are finned only over the discharge region (along the optical axis), and near the ends (window walls) the tubes are bare. In this way cavity temperature uniformity is maintained along the optical axis by only removing the discharge deposited heat. Comparison of performance for various heat exchanger configurations and the affect of the various parameters are most simply performed by making use of non-dimensional flow parameters. Figure 19 gives the shell or laser gas side heat transfer characteristics assumed for this configuration. These characteristics are given in terms of the non-dimensional partameters:

$$St = \frac{h_{gas}}{\rho u c_p},$$

$$\mathrm{Pr} = \frac{\mu c_p}{K_{gas}},$$

$$and\ \mathrm{Re} = \frac{\rho \mu D_h}{\mu}$$

where h_{gas} = gas side heat transfer coefficient, ρ= gas density, μ= gas approach velocity, c_p = gas specific heat capacity, , μ= gas viscosity, k_{gas} = gas thermal conductivity, and D_h = shell side hydraulic diameter.

[1] Kays, W.M. and London, A.L., Compact Heat Exchangers. Third Edition, McGraw-Hill 1984

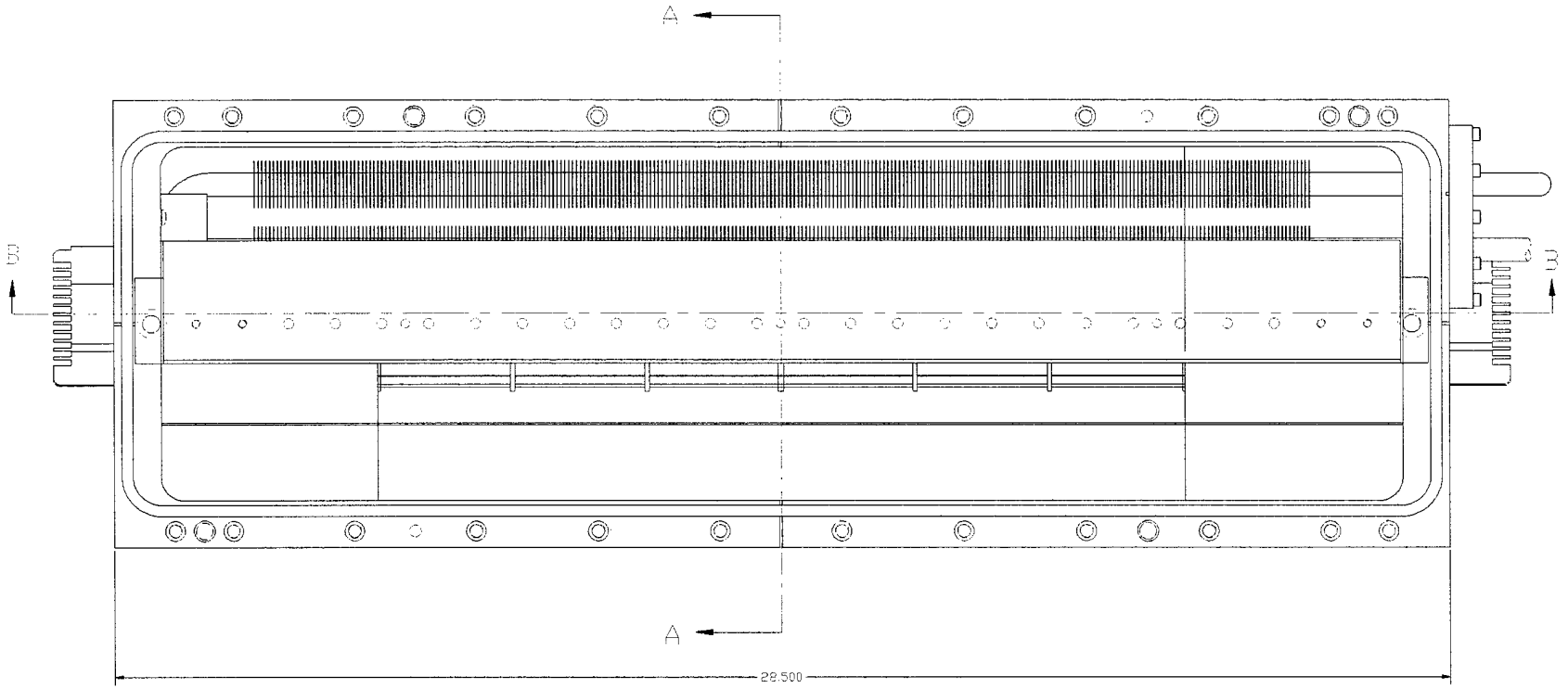

Figure 16. Interface surface Between SRL Flow Subsystem and Cymer Discharge Region

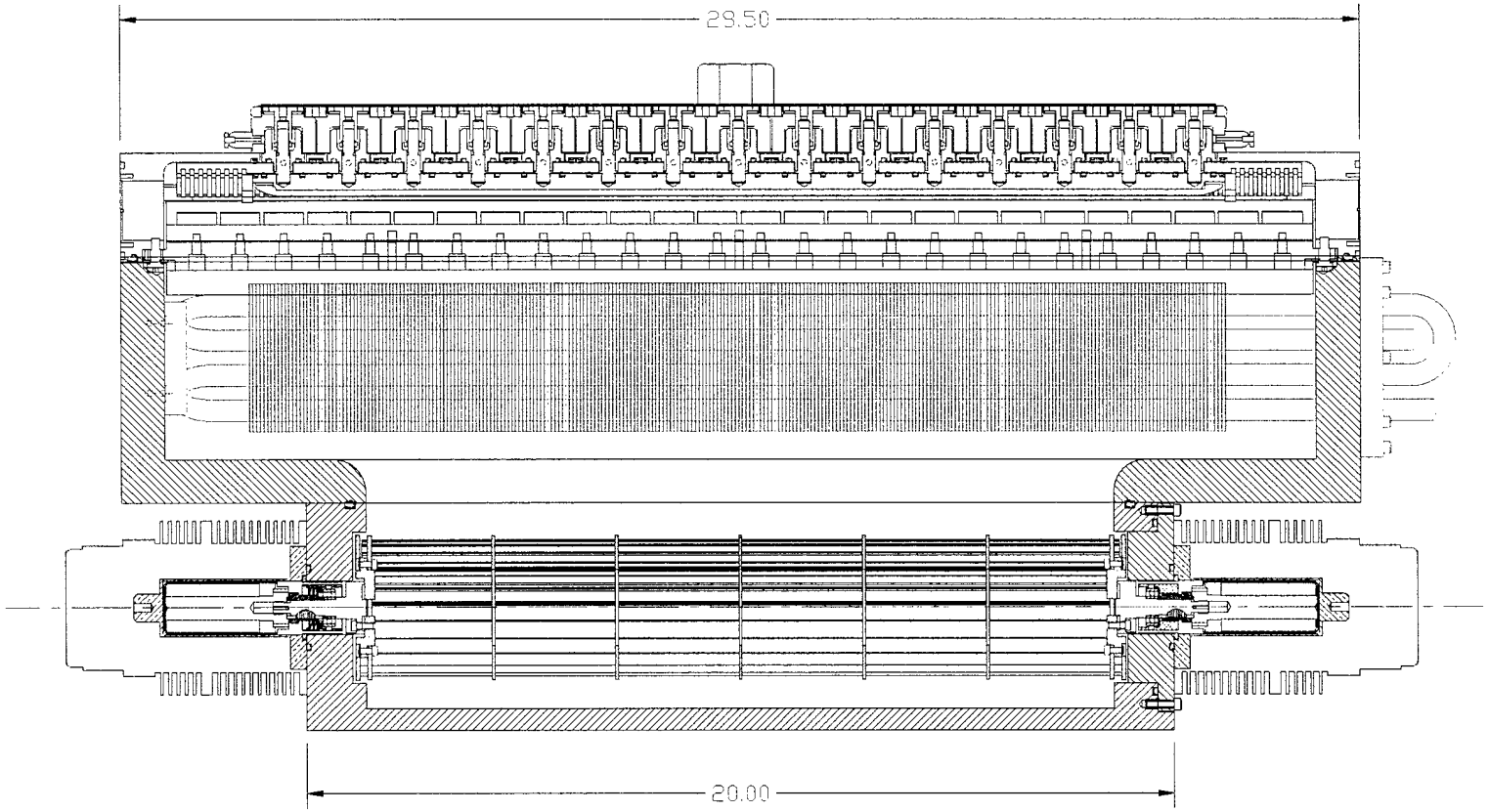

Figure 17. Brassboard Flow Subsystem – Long Section View

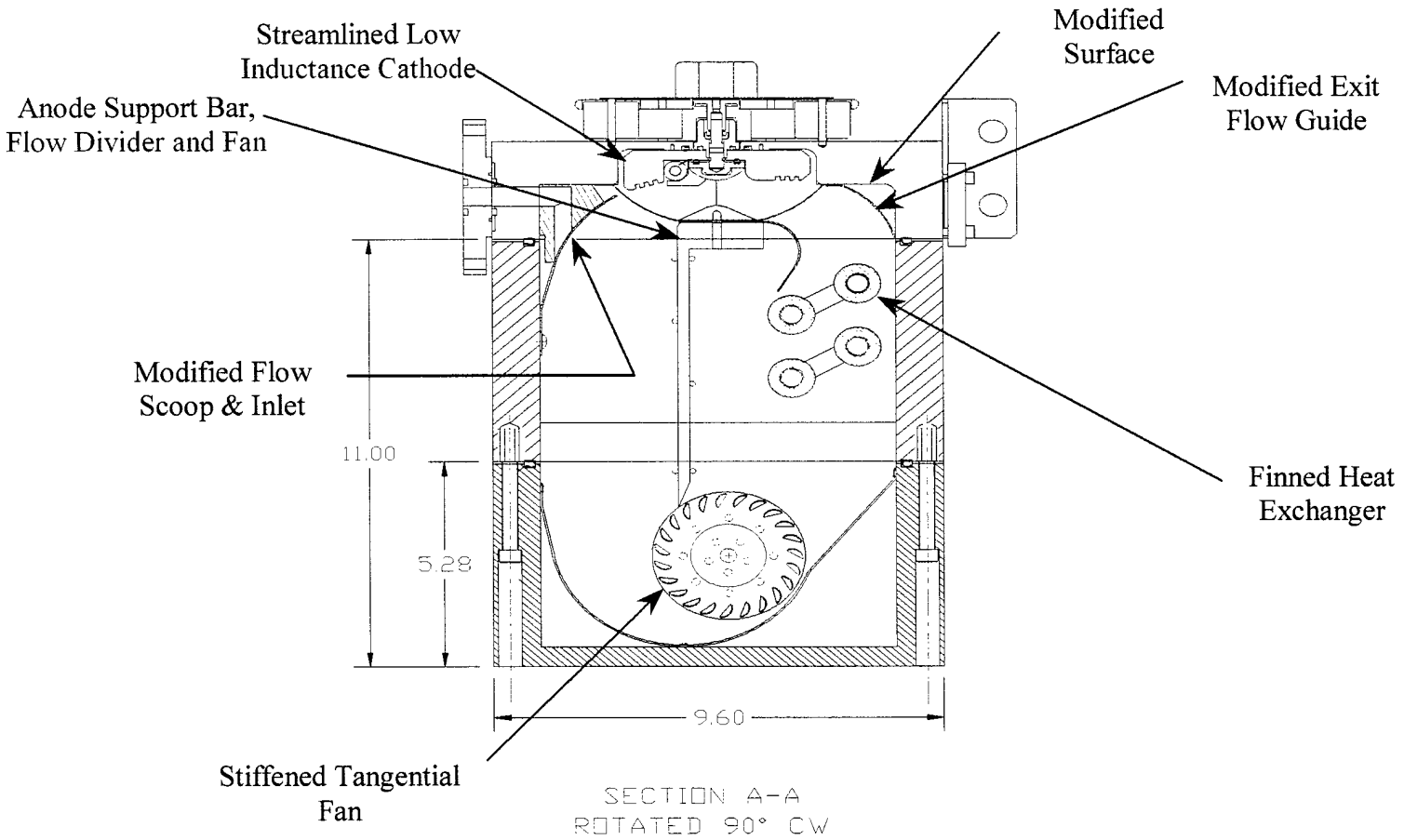

Figure 18. Brassboard Flow Subsystem – Cross Section View

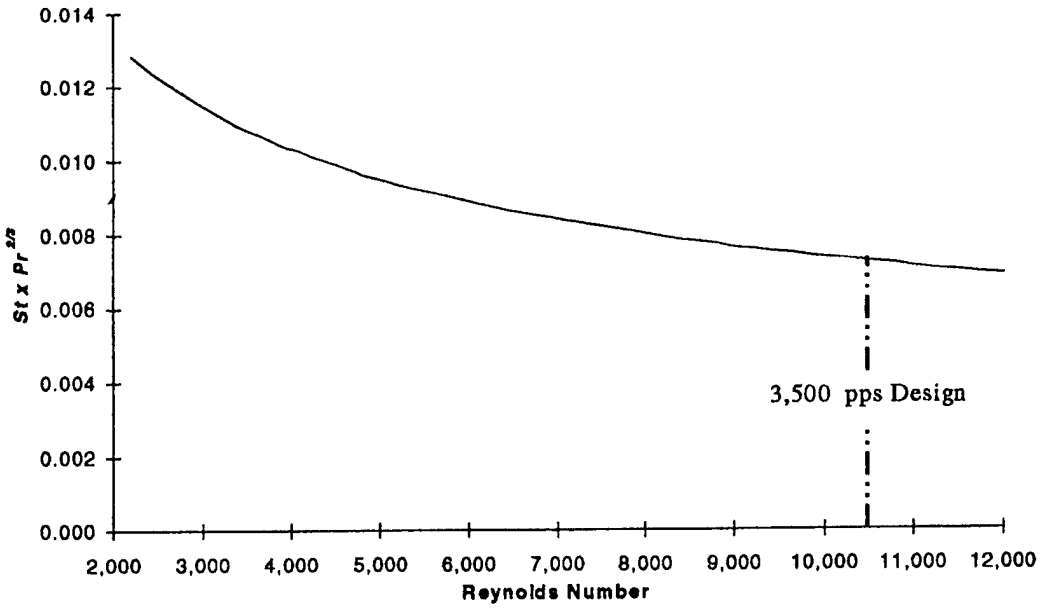

Figure 19. SRL Brassboard Heat Exchanger Characteristics Based on Kay and London[1]

Flow Subsystem Mock-Up Test Development

Two approaches have been pursued to achieve significant increases in laser pulse rate through flow subsystem modifications. The first approach was to explore methods to maximize practical excimer pulse rate with small modifications to the existing Cymer ELS laser series. The second approach was to develop the brassboard design that would develop the full five-fold increase in pulse rate. Both approaches utilized mock-up flow test systems which provided the performance database for the development of an integrated flow subsystem brassboard.

Cymer Flow Model Test Results

The Cymer flow model was delivered to SRL where modifications and tests were carried out. Tests were conducted in the "As Received" configuration at fixed geometry and varying fan speed. The model was then modified to eliminate bypass flow above the cathode; establish more nearly two dimensional flow near the window walls; and allow higher fan speeds by installing the rigid fan wheel as developed by Cymer. These modifications provided an improvement in flow speed of 5.4% and an improvement in fan efficiency of 23%, as shown in Figure 20, and Figure 21.

Cymer completed development of fan fabrication to their own specifications that uses an Aluminum alloy which retains its hardness during brazing and plating operations and is consequently more rigid than earlier models. These "stiffened" fans were employed in the tests conducted on the Cymer ELS Flow model (which include the above SRL modifications) for three cavity discharge heights (6.7 mm, 9.9 mm and 16.7 mm). Test results are shown in figure 22.

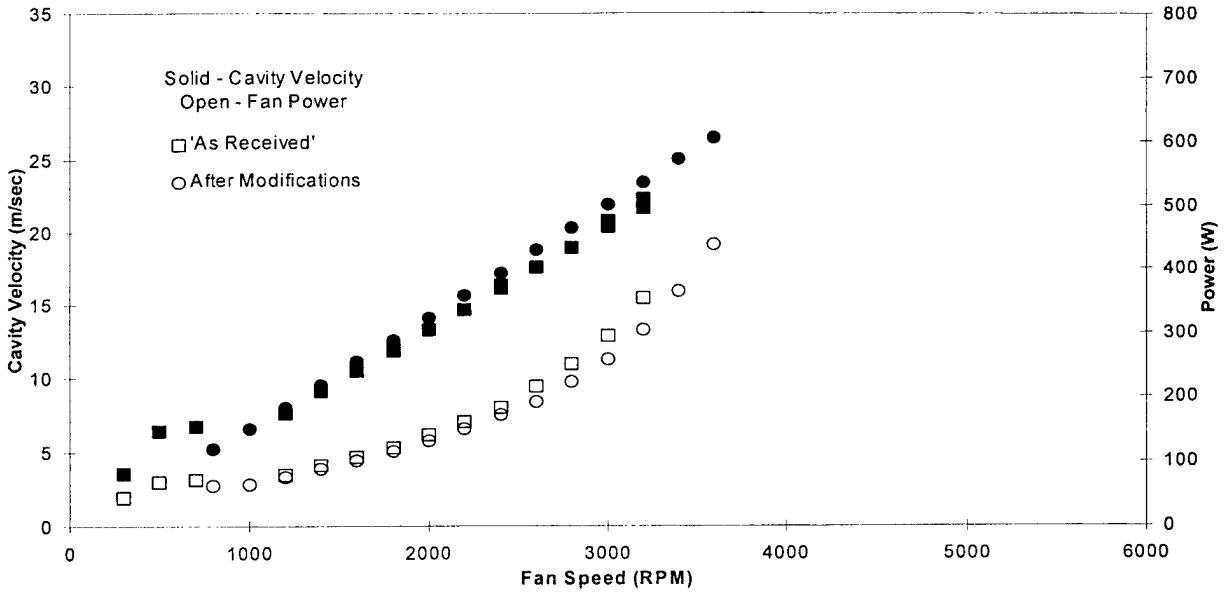

Figure 21. Cymer 3" Flow Model Performance: Fan Efficiency Before and After Modifications

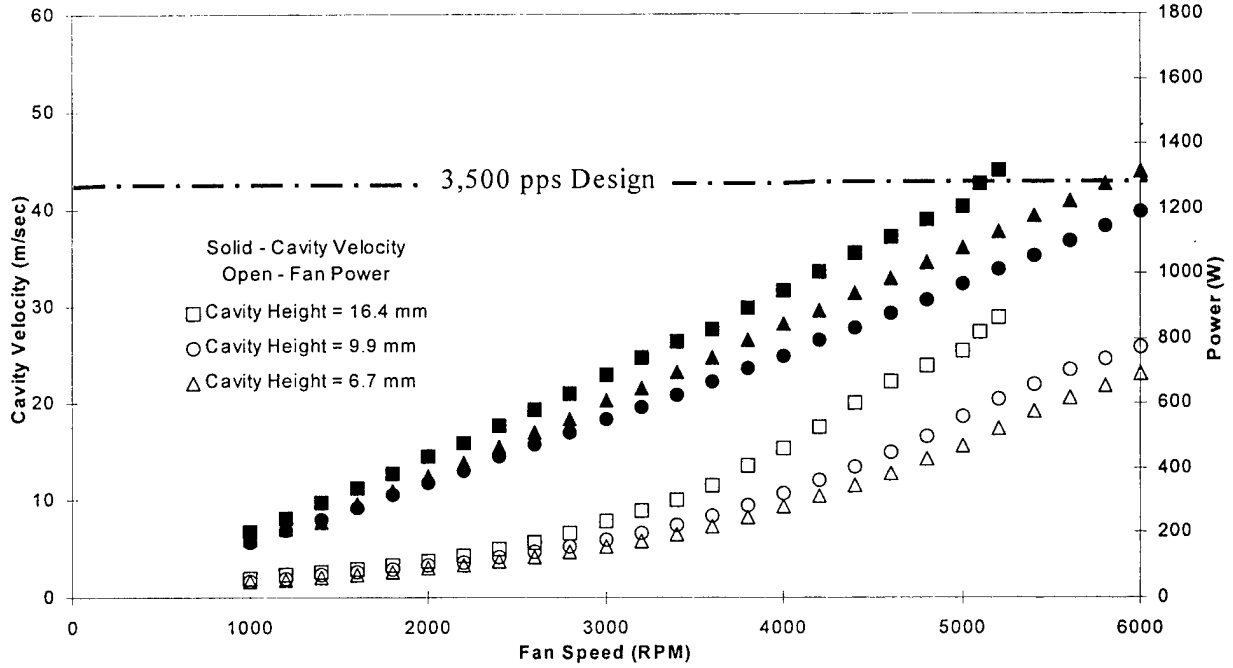

Figure 22: Cymer 3" Flow Model Performance: with "Stiffened" Fan, Cavity discharge Heights of 6.7 mm, 9.9 mm and 16.4 mm.

The required flow velocity of 42.5 m/sec for 3,500 pps operation has been demonstrated for a cavity discharge height of 16.4 mm after the SRL modifications. However, the Cymer flow subsystem has insufficient space for a heat exchanger to remove the required heat loading given in Table 1. Also, cavity flow velocity variations indicate that stall occurs over a significant portion of the fan and that the stall regions shift in time for off-design operation. Tests performed for a discharge height of 9.9 mm and with the heat exchanger removed, as shown in Figure 23, demonstrate this phenomenon clearly.

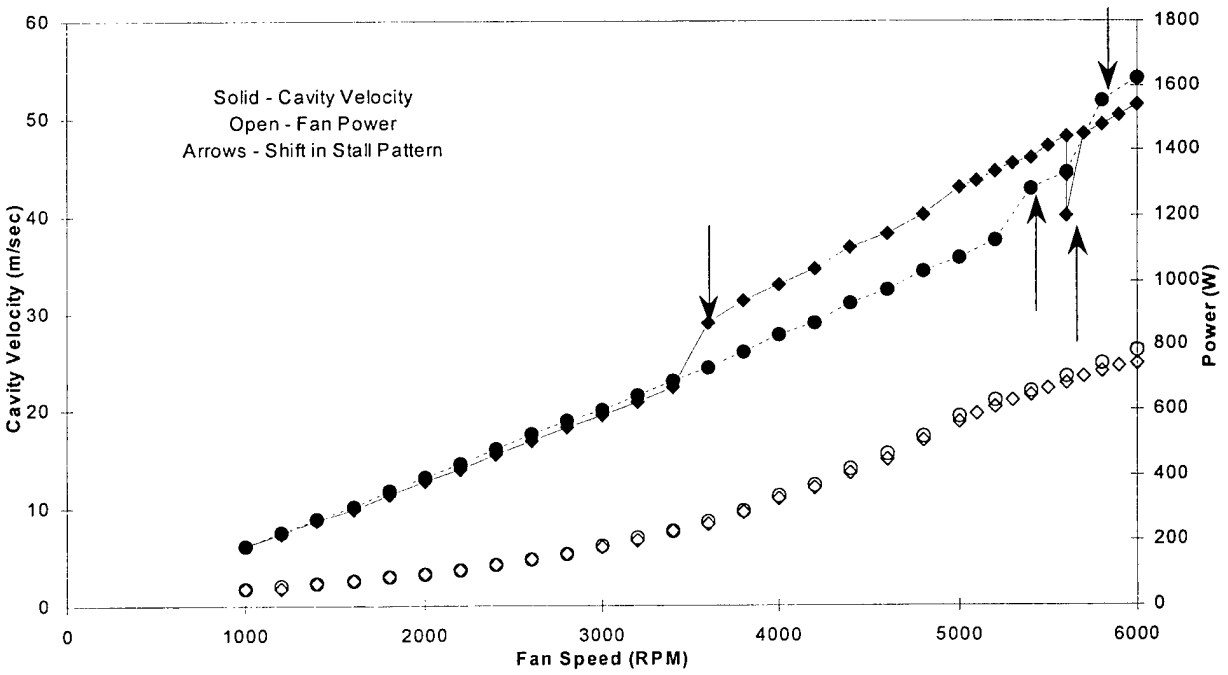

Figure 23. Cymer 3" Flow Model Performance: with "Stiffened" Fan, No Heat Exchanger, Discharge Height of 9.9 mm.

SRL Brassboard Flow Model: Flow Performance and Scaling.

The SRL Brassboard Flow Model was designed and built to test the SRL concept based on the original 6.7 mm cavity discharge height program approach. A fan whose length is significantly shorter than the laser discharge length was chosen. A 3-segment or 9.1" long fan made from a Cymer 26.5" long "stiffened" fan was utilized.

Tests on the SRL Brassboard Flow Model configured with the Cymer ELS Flow Model Head, as shown in Figure 24, and a shortened, "stiffened" fan was performed with the three cavity discharge heights of 6.7 mm, 9.9 mm and 16.4 mm. The SRL Brassboard Flow Model was configured with the Cymer ELS heat exchanger, and single Cymer fan motor. Test results in Figure 25 show that velocity measured at the center of the optical axis varies linearly with fan

speed and the affect of discharge height is slightly noticeable at the higher fan speeds. However, comparison of the velocity profiles, shown in Figure 26, along the cavity centerline for the three discharge heights indicate that there is significant velocity roll-off for the larger discharge heights. This shows that the shorter fan is not suited for the larger cavity discharge heights.

The SRL Brassboard Flow Model was modified to include the longer 17.1" long, stiffened fan. The extended fan length was necessary to optimize the brassboard design to the baseline cavity discharge height of 16.5 mm. Test results comparing the performance of the SRL Brassboard Flow Model re-configured for the 6-segment fan with the configuration for the 3-segment fan are shown in Figure 27 and Figure 28. The velocity uniformity for the cavity discharge height of 16.5 mm, defined as $(u_{max} - u_{min})/ u_{mean}$ over the cathode length, is 16.1% for the longer (6-segment) fan compared to 77.2% for the shorter (3-segment) fan. These results show that flow performance is improved and flow uniformity along the optical axis is significantly improved.

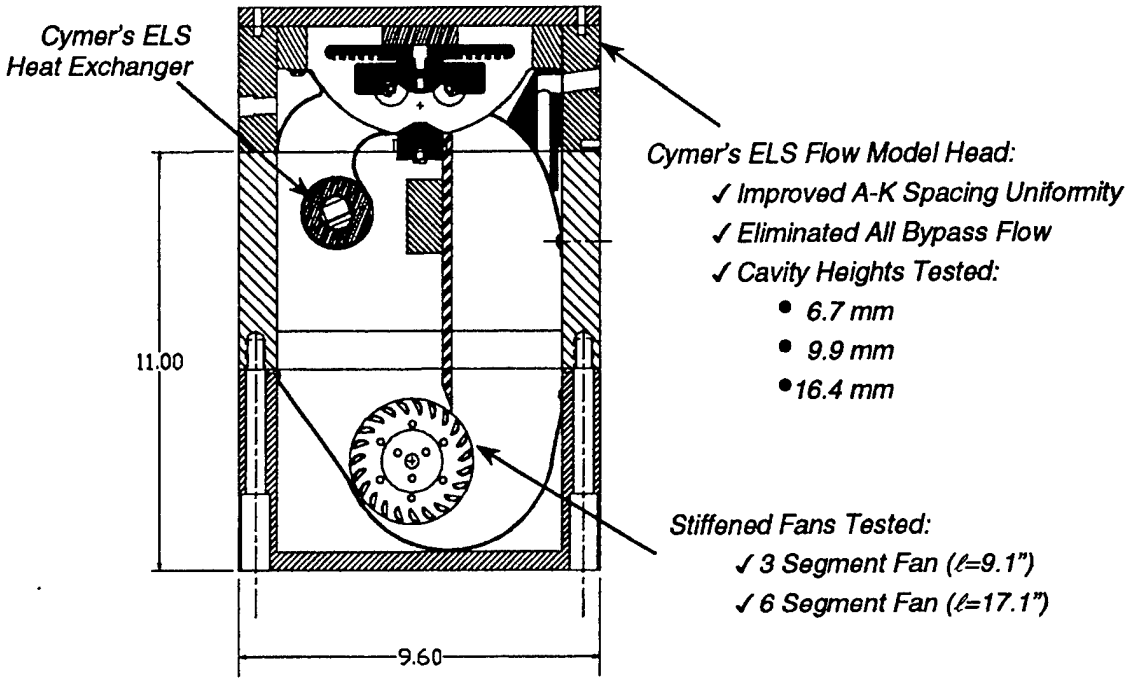

Figure 24. Brassboard Flow Model Configured with Cymer ELS Flow Model Head, Cymer ELS Heat Exchanger and Single Cymer Motor.

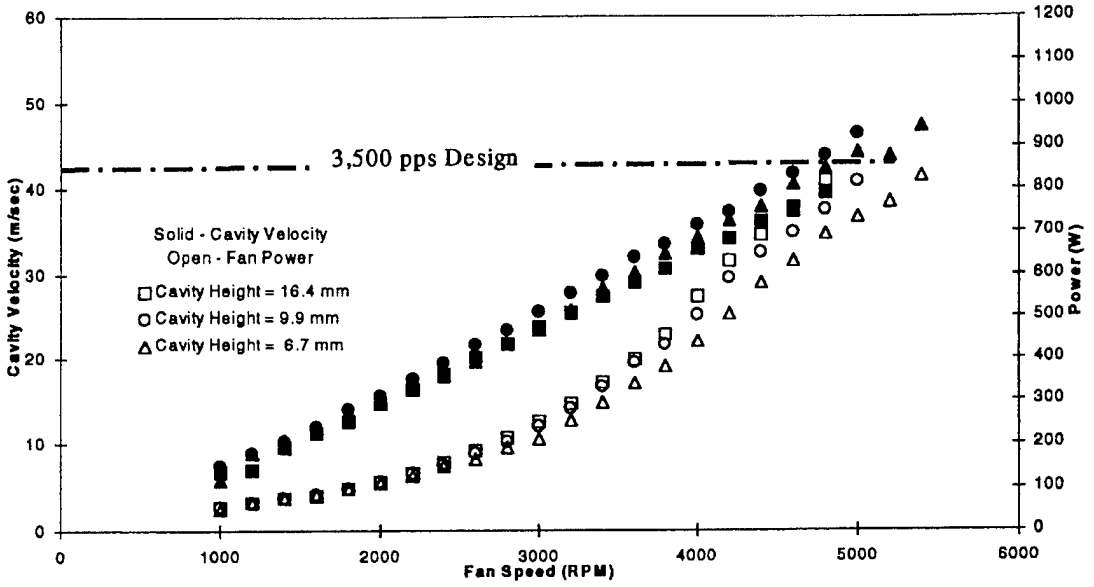

Figure 25. Brassboard Flow Model Performance: with Cymer ELS Flow Model Head, Cymer ELS Heat Exchanger, single Cymer Motor, 3-Segment Fan, and Three Cavity Discharge Heights

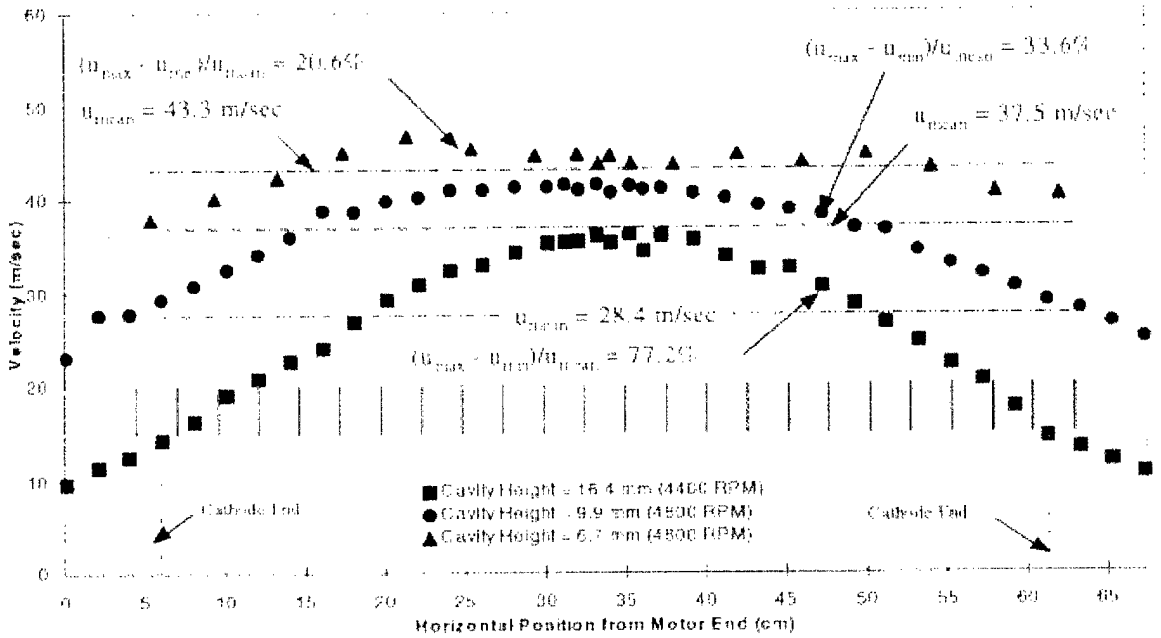

Figure 26: Velocity Profiles along Optical Axis of Brassboard Flow Model: with Cymer ELS Flow Model Head and Heat Exchanger, single Cymer Motor, 3-Segment Fan, and Three Cavity discharge Heights

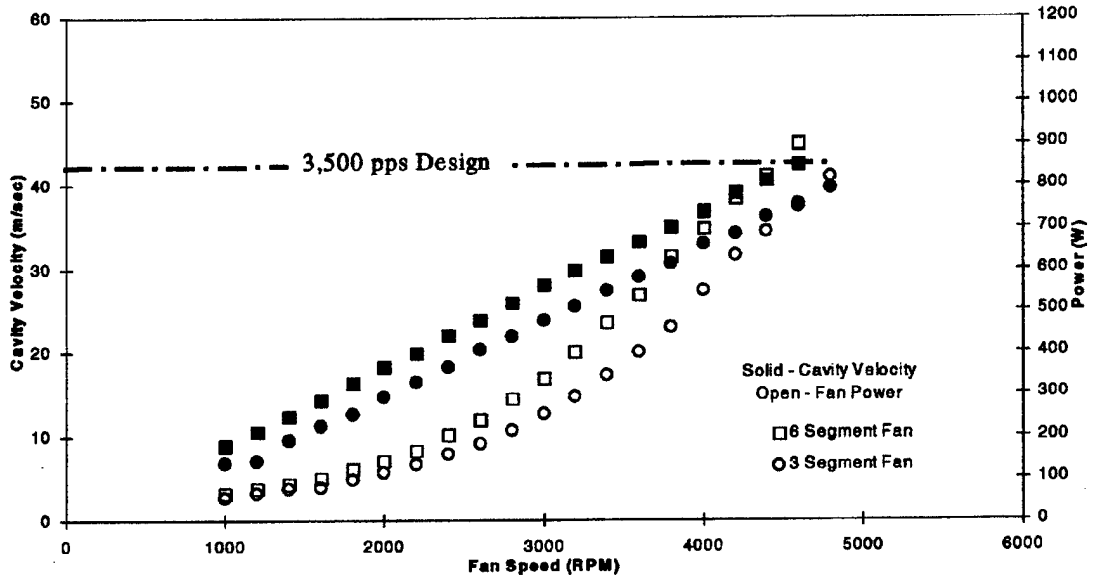

Figure 27. Brassboard flow Model Performance: with Cymer ELS flow Model Head, Cymer ELS Heat Exchanger, single Cymer Motor, 16.4mm Cavity Discharge Heights, and Two Fan Lengths.

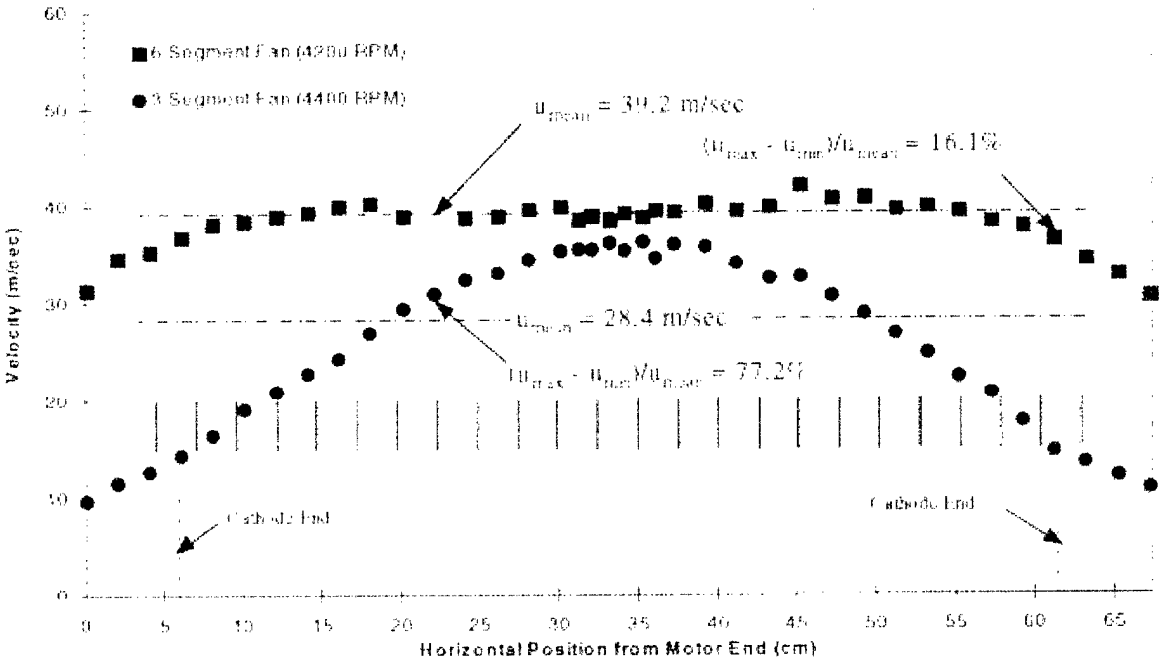

Figure 28. Velocity Profiles along Optical Axis of Brassboard flow Model: with Cymer ELS Flow Model Head and Heat Exchanger, single Cymer Motor, 16.4 mm Cavity discharge Heights and Two fan Lengths.

Modifications to the SRL Brassboard Flow Model were then made to include the SRI heat exchanger design. The heat exchanger design chosen, as shown in Figure 29, consists of four finned tubes with a fin OD of 1.00", and tube OD of 0.50".

Performance comparison of the brassboard flow model with the extended fan length 01 17.13 in. and (1) no heat exchanger installed, (2) the Cymer ELS heat exchanger installed and (3J the larger SRL heat exchanger are given in Figure 30. For the baseline discharge height of 16.5 mm, the design cavity flow speed of 42.5 m/sec is achieved at a fan speed of 4200 rpm and a fan motor power demand of 880 W in air (this scales to 2500 W in excimer laser gas) for all three cases. These results show that there is no significant added burden to the fan since the Brassboard design provides adequate space for a larger heat exchanger.

These test results along with the Cymer Flow model test results presented in the previous section indicate that there is an optimal tangential fan length for a particular cavity discharge height. Cymer Flow Model tests with a discharge height of 9.9 mm show that stall occurs over a significant portion of the fan and that the stall regions shift in time for off-design operation. Therefore, too long of a fan has undesirable effects. The SRL Brassboard Flow Model results presented above show that flow uniformity along the optical axis for the larger cavity discharge heights are better with the 6-segment fan.

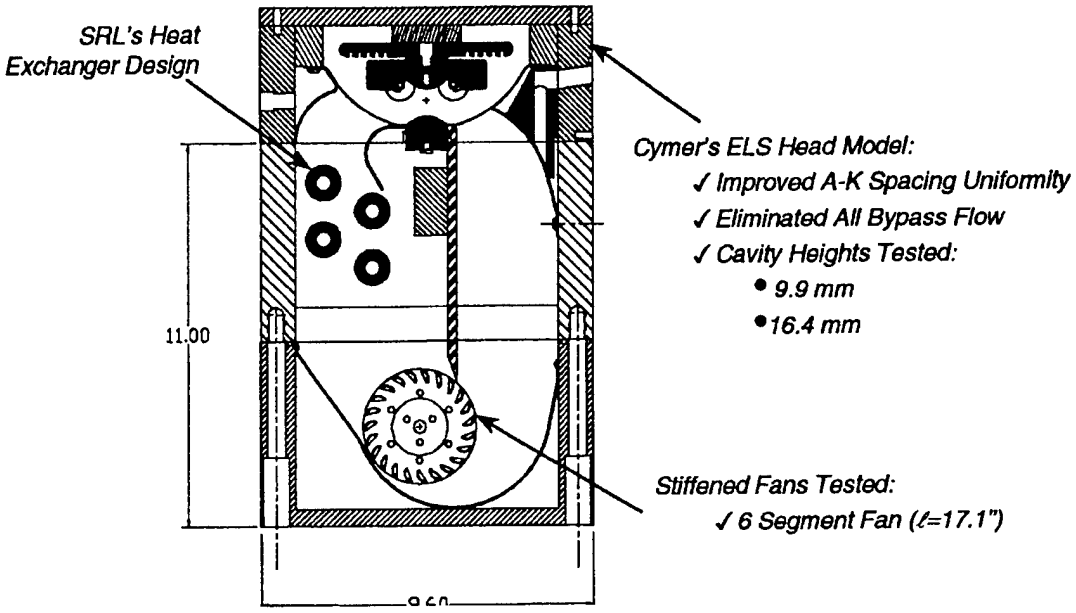

Figure 29. Brassboard Flow Model with the Cymer ELS Head and Larger SRL heat Exchanger.

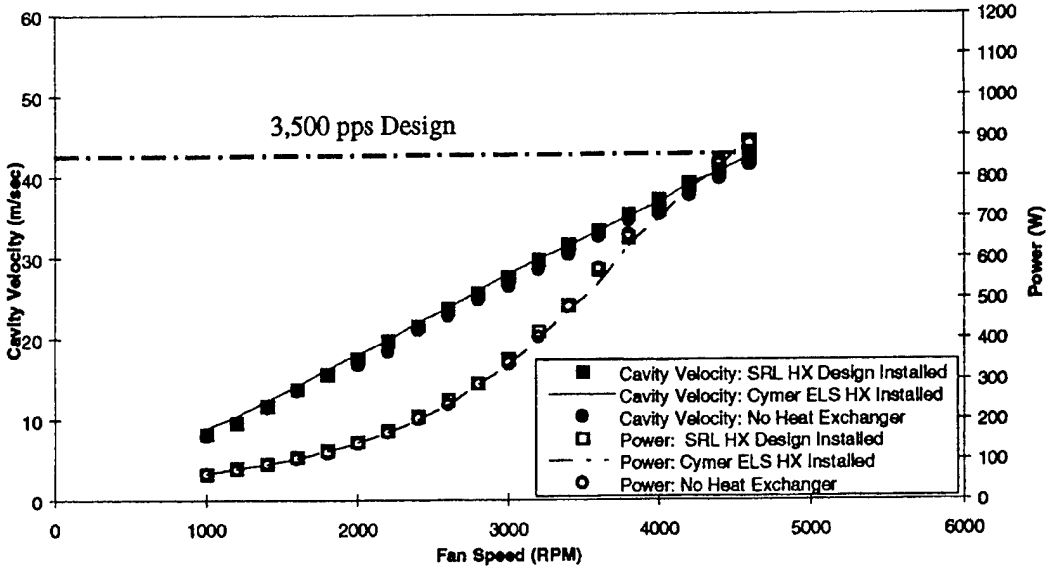

Figure 30. SRL Brassboard Flow Model Performance with fan Length of 17.13" and 16.5 mm Cavity discharge

These results also indicate that in the SRL Brassboard design the lack of or presence of a heat exchanger places no significant burden on the fan. This suggests that the SRL Brassboard design has sufficient space to accommodate an even larger heat exchanger subsystem.

SRL Brassboard Flow Model: "Streamlined" Low Inductance Head Test Results.

The SRL Brassboard Flow Model has been modified to include a streamlined approximation of Cymer's "low inductance" head design as shown in Figure 31. The inlet flow guide and flow scoop have been modified to provide a smooth transition to the cathode insulator. The upstream section of the cathode insulator has been shaped to provide a reasonably smooth flow wall between the inlet flow guide and the cavity. The exit flow guide has been modified and a spacer has been added also to provide smooth flow wall. It was not necessary to preserve details of these wall segments in the fmal design. It was sufficient to provide comparable wall smoothness.

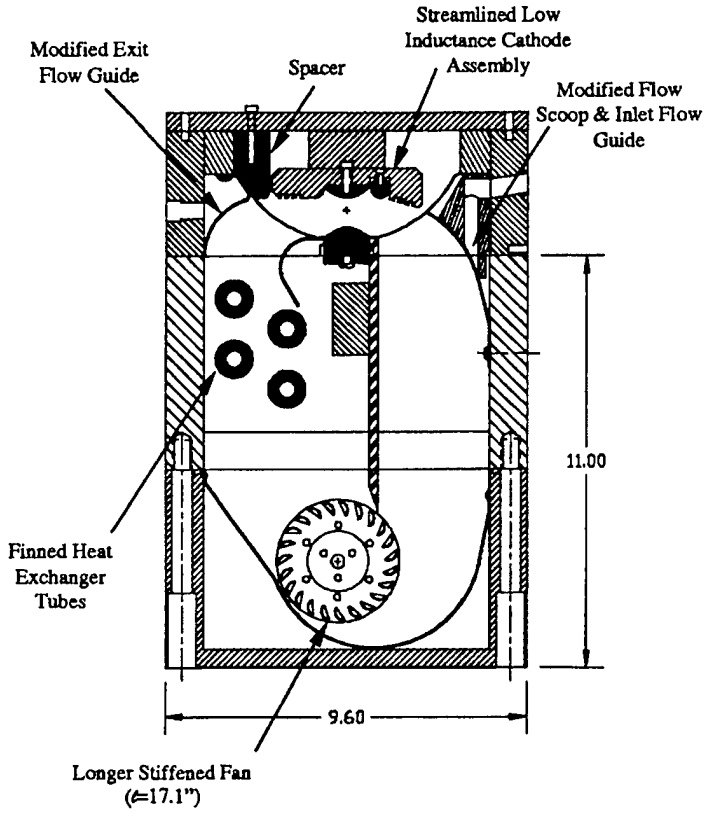

Figure 31. Brassboard Flow Model with "Streamlined" Low Inductance Laser Head and SRL Heat Exchanger.

Tests on the re-configured SRL Brassboard Flow Model have been performed with the baseline cavity discharge height of 16.5 mm. Results are compared with those for the ELS discharge head, prior to these cathode side modifications, in Figure 32 and Figure 33. At any given fan speed and fan power demand, cavity gas velocity is slightly higher in the new configuration. Cavity flow uniformity with the streamlined low inductance head is also slightly

improved as shown in Figure 33. There is still some flow speed roll off near the cathode. The design cavity flow speed of 42.5 m/sec is now achieved at a fan speed of 4400 rpm and a fan motor power demand of 832 W in air, which would scale to excimer operation by the density ratio a (see Table 3) to 1897 W.

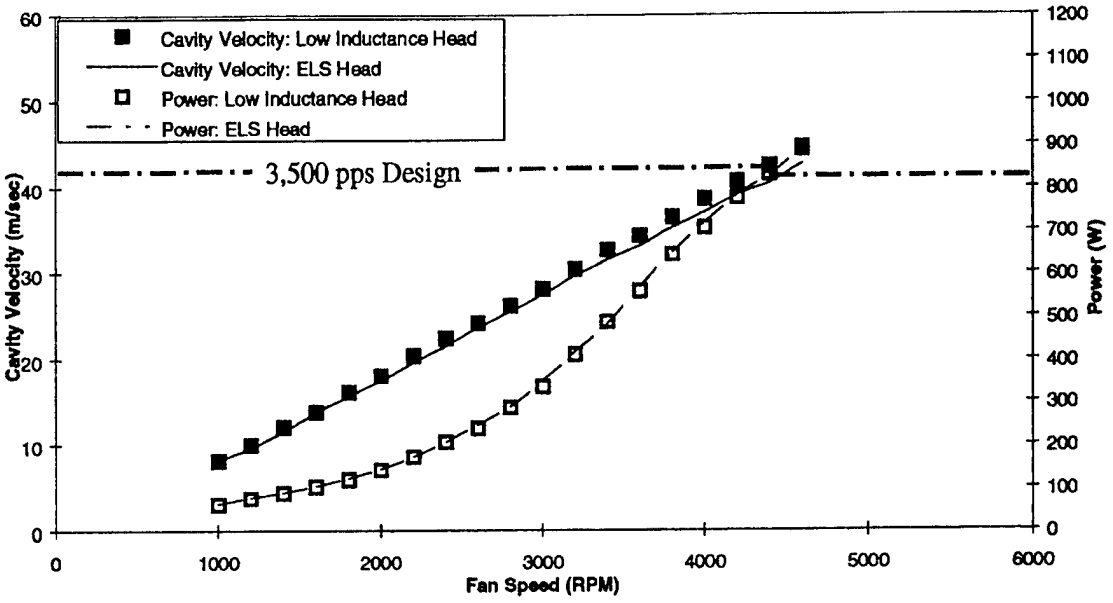

Figure 32. SRL Brassbord Flow Model Performance with Streamlined Low Inductance Head. Compared with ELS Head.. (Cavity discharge Height is 16.5 mm)

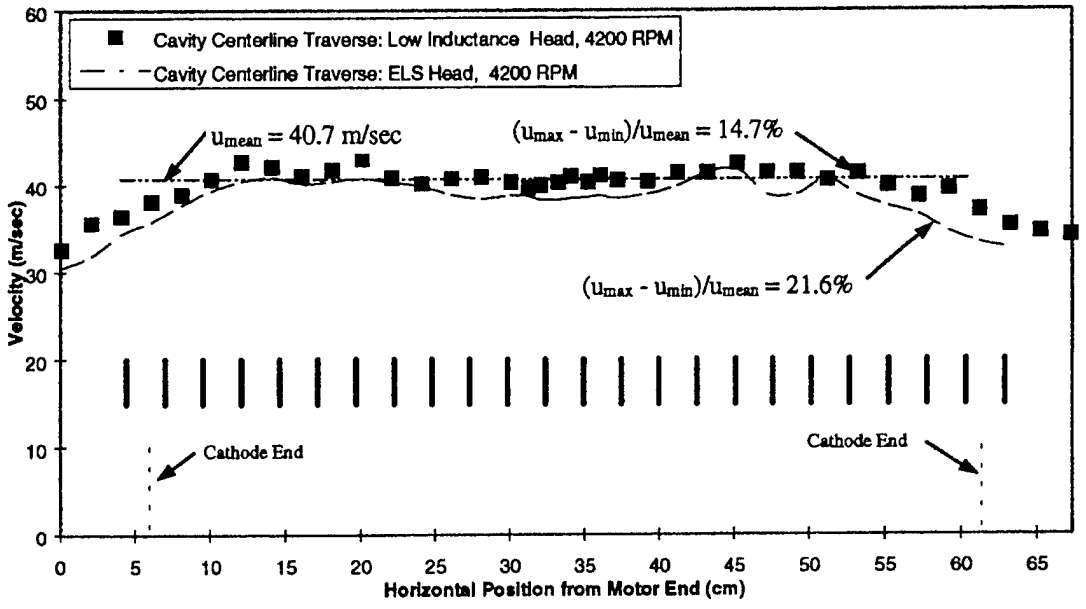

Figure 33. Velocity Profiles along Optical Axis of Brassboard Flow with Streamlined Low Inductance Head, Compared with ELS Head. (Cavity Discharge Height is 16.5 mm)

SRL Brassboard Flow Model: Single 3 HP Motor Test Results.

All of the test results presented thus far in this report have been performed with "room air" (air at atmospheric pressure and 25°C). Typical fan scaling relations have been used to predict flow performance with the laser gas at the baseline design pressure and temperature from the "room air" test results. Test results presented in this section have been performed using Freon R-22 and CO_2 at atmospheric pressure and varying temperature to simulate laser gas density and discharge loading over a range of operating pressures

These tests were done with the streamlined approximation of Cymer's "low inductance" head and a cavity discharge height of 16.5 mm. Tubular heaters, as shown Figure 34, were used to simulate heating of the flow due to electrical discharge. The tubular heaters consisted of six 0.315-in. diameter resistive elements. These tubular heaters were present for all of the tests presented in this section.

The SRL Brassboard Flow Model was re-configured with a single 3-hp motor, as shown in Figure 34 to allow flow testing and heat exchanger subsystem testing at higher gas density (and flow power demand) to simulate the laser gas at operating pressure and temperature. Due to the larger fan power demands, the higher gas density tests could not be performed with the single Cymer motor. Ideally these test would have been performed using the dual Cymer motor configuration, however, use of the single 3-hp motor configuration was necessary as an intermediate step because of a number of difficulties initially encountered in trying to achieve dual Cymer motor operation.

Tests on the SRL Brassboard Flow Model configured with the single 3 Hp motor and tubular heaters were first performed with air at atmospheric pressure and the baseline cavity discharge height of 16.5 mm. Results are compared in Figure 35 and Figure 36 with those of the same flow model but with the single Cymer motor configuration. At any given fan speed, cavity gas velocity is slightly lower with the single 3 HP motor. Power demand is significantly lower for fan speeds above 2800 RPM and correspondingly fan efficiencies are much higher. Also, fan power demand for the 3 hp motor follows the typical fan scaling laws, namely that $power \propto (speed)^3$.

Flow tests were conducted to verify that the tubular heaters did not significantly affect flow performance. Rods of the same diameter as the tubular heaters were installed in the Brassboard Flow Model and flow tests have verified that they do not significantly affect flow performance. As expected, cavity flow uniformity was further improved by the insertion of the rods. We concluded that the heater rods in the configuration of Figure 34 are suitable for simulating the average discharge power deposition specified in Table 3 without significantly altering brassboard flow conditions.

Velocity Profiles Transverse to Optical Axis

Tests have been performed to determine cavity velocity uniformity between cathode and anode over a 16.5 mm discharge height in the SRL Brassboard Flow Model with the single 3 hp motor. Hot wire velocity measurements were made at the cavity center transverse to the optical axis, from the anode to the cathode. Power spectral

densities in Figure 37 show broad, low frequency spectra with peaks at fan rotational speeds. The turbulence power spectrum is concentrated at frequencies below 200 HZ, which is well below the flow transit time through the discharge region. Therefore the velocity fluctuations appear as variations in mean velocity rather than turbulence in the conventional sense. Results in Figure 38 show excellent spatial velocity uniformity, RMS velocity fluctuations of 15% near the anode and less than 7.5% elsewhere.

Higher Gas Density Flow Performance

The SRL Brassboard Flow Model was filled with Freon R-22 and with CO_2 at atmospheric pressure to simulate the laser gas at 3.6 atm., 55°C, and corresponding laser gas density, P_{design}, of 2.70 kg/m^3. Test results are compared with those of the flow model filled with air, Freon R-22 and CO_2 in Figure 39 and Figure 40. At any given speed, cavity gas velocity is somewhat higher for freon and CO_2. The fan power demand with freon and CO_2 was scaled with (divided by) the density ratio, a as given in Equations (1), to obtain the "air equivalent" power demand. Other pertinent scaling parameters are also given in Equations (1). Figure 39 shows agreement of the air equivalent power demand and the fan power demand for air. In other words, fan power demand scales directly with gas density, although flow velocity and therefore, fan efficiency is higher at higher gas density as shown in Figure 40.

SRL Brassboard Flow Model: Heat Exchanger Subsystem Tests

Tests of the heat exchanger subsystem as shown in Figure 41 have been performed in the SRL Brassboard Flow Model, as shown in Figure 34, filled with air and CO_2. Heating of the flow due to electrical discharge was simulated in the tests with six 0.3 15 in. diameter tubular heaters as shown in Figure 34. The test results shown in Figure 42 give the heat exchanger performance in terms of non-dimensional parameters.

Comparison of the heat exchanger test results with the performance curve (solid curve) assumed to be representative for the heat exchanger configurations of interest during the initial design phase is shown Figure 42. The dashed curve in Figure 42 represents a best fit to the test data and was used as the basis in the design of the heat exchanger subsystem for the Brassboard as shown in Figure 17 and Figure 18. Based on these test results, the predicted performance of the Brassboard Heat Exchanger subsystem is given Table 4.

Heat exchanger subsystem tests also included measurements of cavity temperature variations along the cavity optical centerline. Test results with a fan speed of 4800 RPM and with the tubular heaters off (air temperature maintained at ~ 25°C) are shown in Figure 43 and with the tubular heaters on (air temperature maintained at ~ 50°C) are shown in Figure 44. Results show excellent temperature uniformity at the design cavity flow velocity.

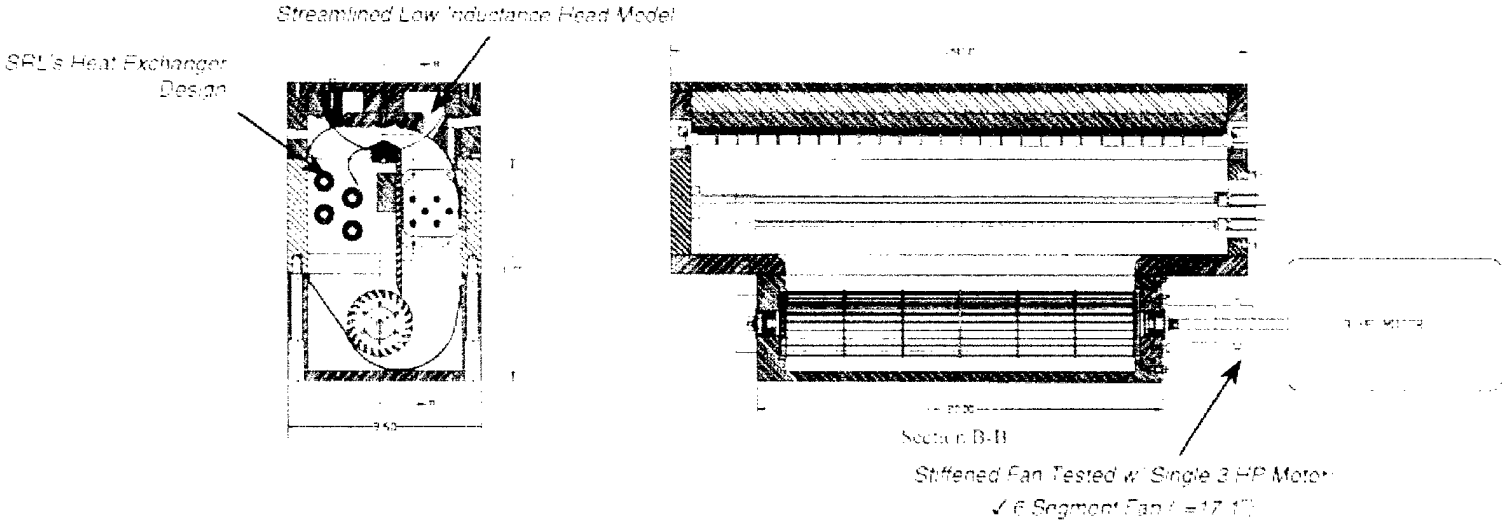

Figure 34. Brassboard Flow Model with Single 3 hp Motor, SRL Heat Exchanger Design and "Streamlined" Low Inductance Head

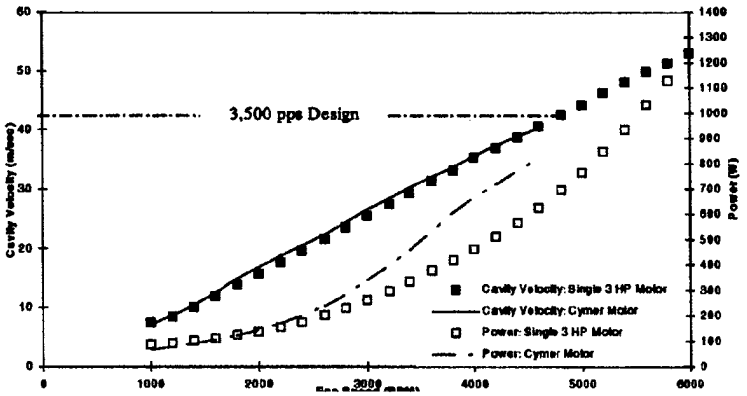

Figure 35. Brassboard Flow Model Performance with single Cymer Motor and 3 Hp Motor

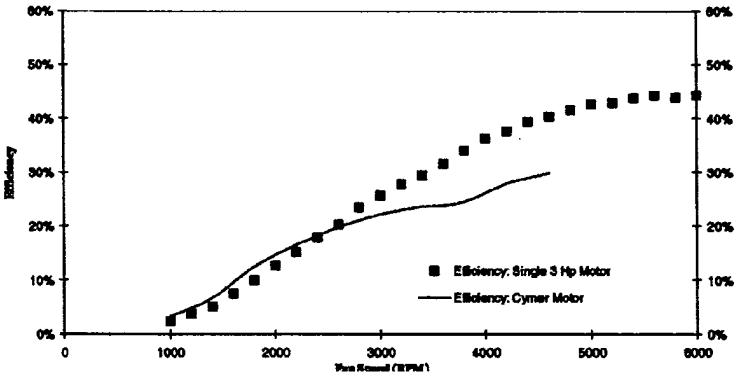

Figure 36. Brassboard Flow Model Performance: Efficiency with Single Cymer Motor and 3 Hp Motor

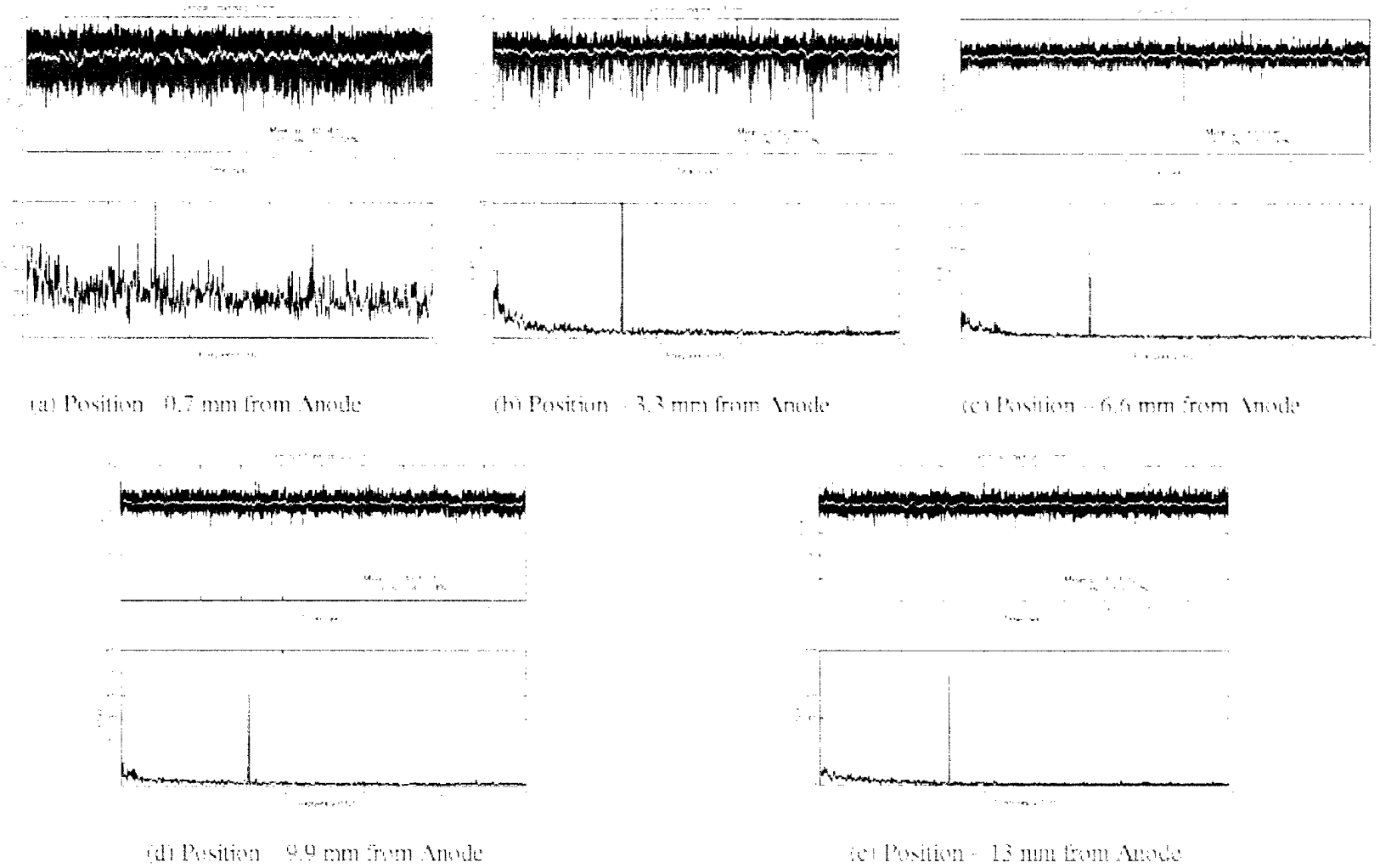

Figure 37. Temporal Velocity Variations and Power Spectral Densities at Various A/K Stations at a Fan Speed of 4800 RPM

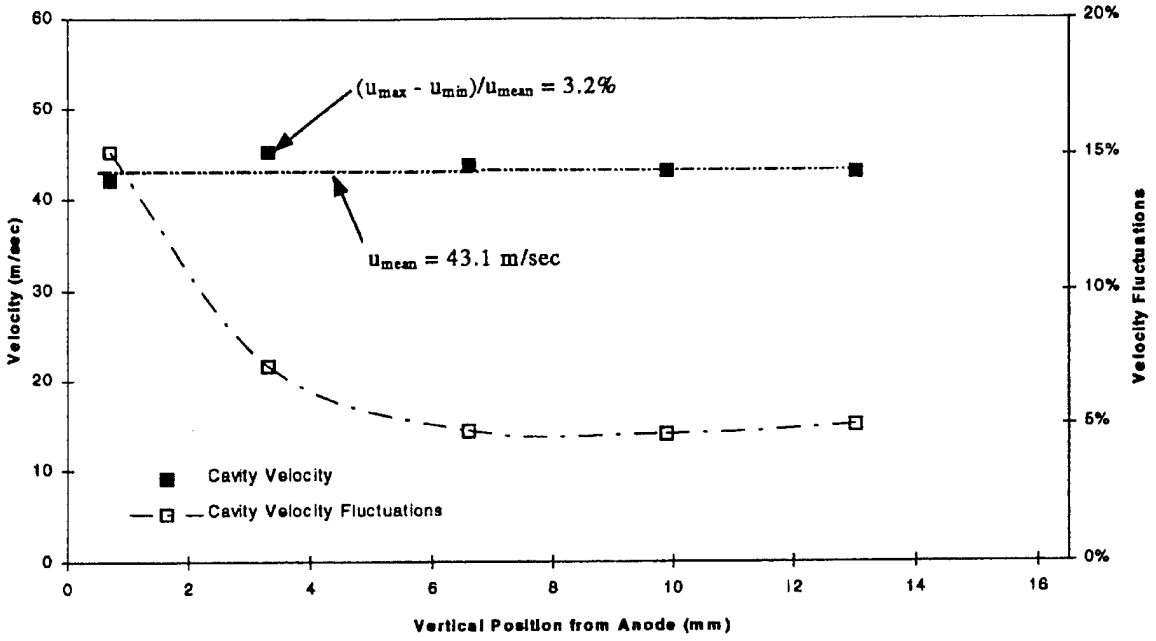

Figure 38. Velocity profile from the Anode to the Cathode at the Center of Optical Axis

$$
\begin{array}{lll}
Molecular\ Weight_{freon} = 86.47 & Molecular\ Weight_{CO_2} = 44.01 & Molecular\ Weight_{air} = 28.97 \\
\rho_{freon}/\rho_{design} = 1.31 & \rho_{freon}/\rho_{design} = 0.67 & \rho_{air}/\rho_{design} = 0.44 \\
\sigma = \rho_{freon}/\rho_{air} = 2.98 & \sigma = \rho_{CO_2}/\rho_{air} = 1.52 & Re_{air}/Re_{design} = 0.8 \\
Re_{freon}/Re_{design} = 3.34 & Re_{CO_2}/Re_{design} = 1.50 &
\end{array}
\qquad (1)
$$

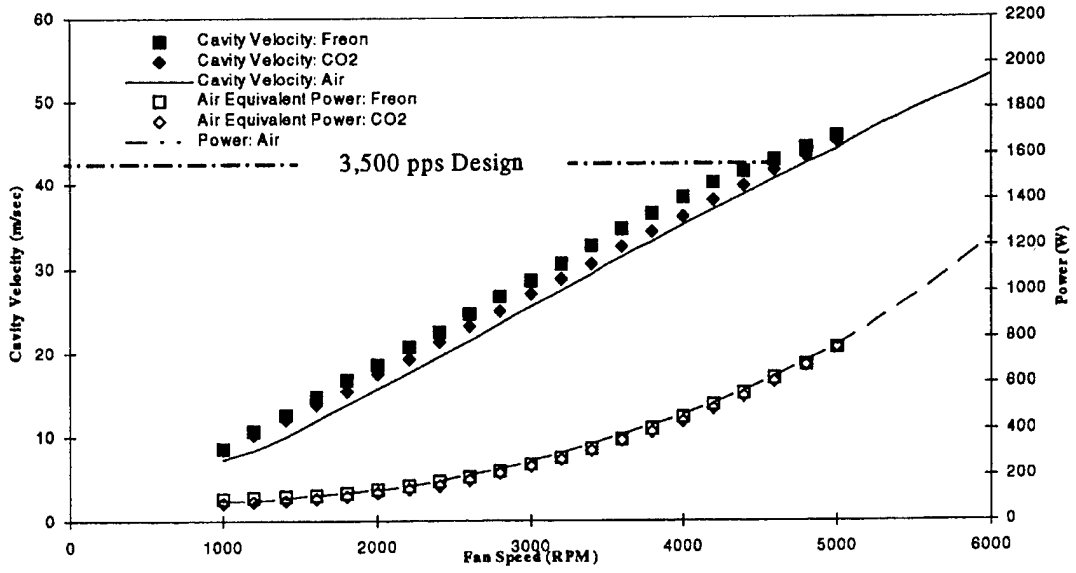

Figure 39. SRL Brassboard Flow Model Test Data: Compression of Model filled with Air, CO_2 and Freon

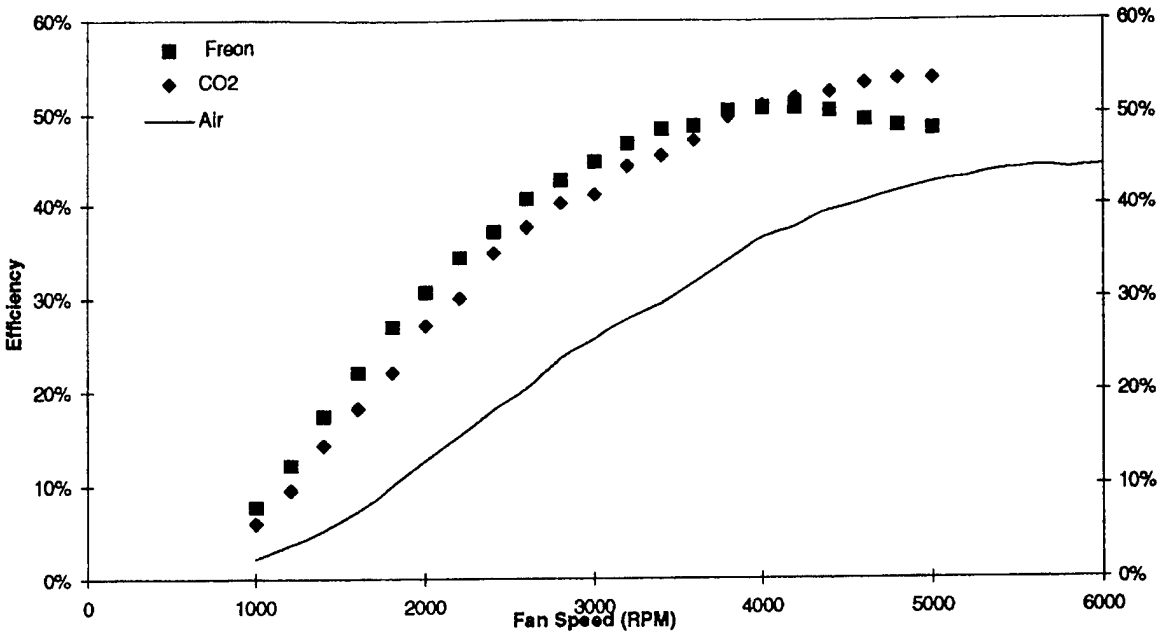

Figure 40. SRL Brassboard Flow Model Fan Efficiency Data: Comparison of Model filled with Air, CO_2 and Freon

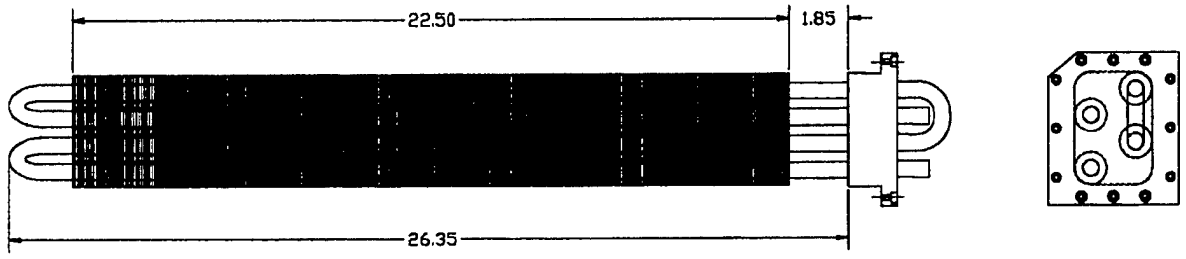

Figure 41. SRL Brassboard Heat Exchanger Design

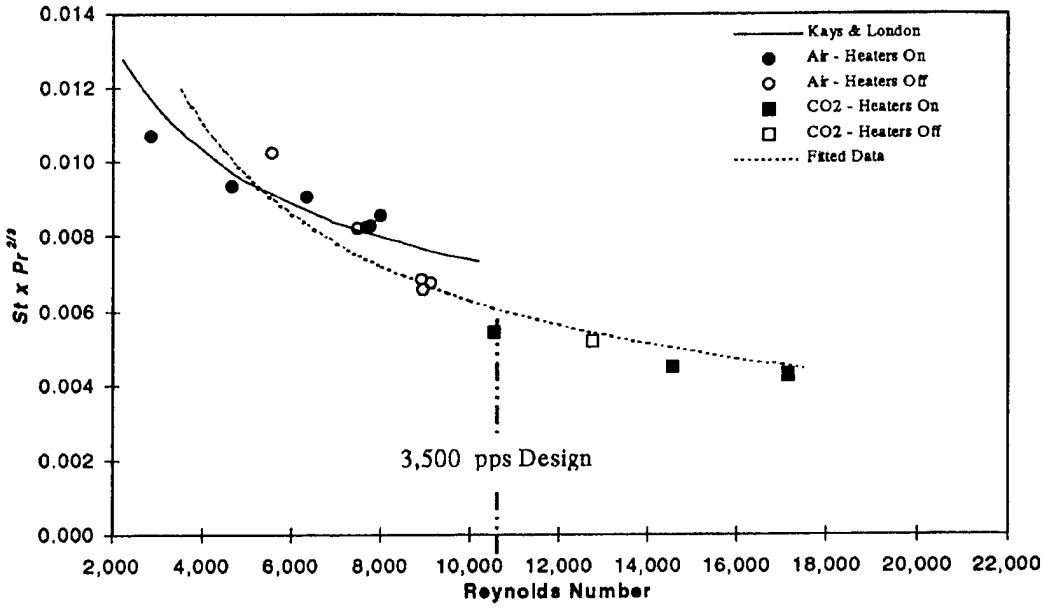

Figure 42. Heat Exchanger Subsystem Test Results: SRL Brassboard Model Filled with and CO_2

Table 4. Brassboard Heat Exchanger Performance

Total Heat Removal Required (W)	**12,390**
Fan Power Demand (W)	1,890
Deposited Electrical Power (W)	10,500
Heat Exchanger Specifications:	
Fin Density (fins/in.)	16
Fin Thickness (in.)	0.0 14
FinOD(in.)	1
Tube OD (in.)	0.5
Shell-Side (Laser Gas):	
Cavity Flow Speed (m/sec)	42.5
Volumetric Flow (cfm)	849
Pressure (Atmospheres)	3.6
Cavity Temperature (°C)	55
Density (kg/m^3)	2.70
Gas AT Across HX (°C)	11
Pressure Drop (in. H_2O)	2.8
Tube-Side (Water):	
Volumetric Flow (gpm)	10
Pressure Drop (psid)	18
Inlet Temperature (°C)	17
Exit Temperature (°C)	21.7

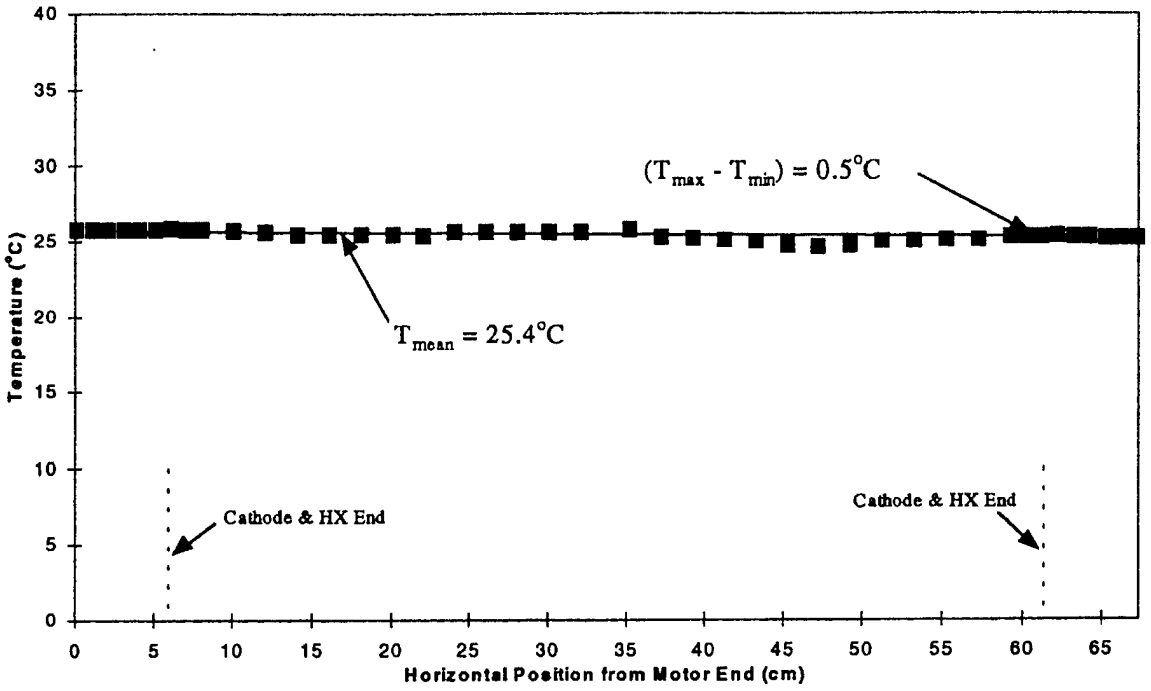

Figure 43. Temperature Profiles along Optical Axis of Brassboard Flow with Room Temperature Air. (Cavity Discharge Height is 16.5 mm)

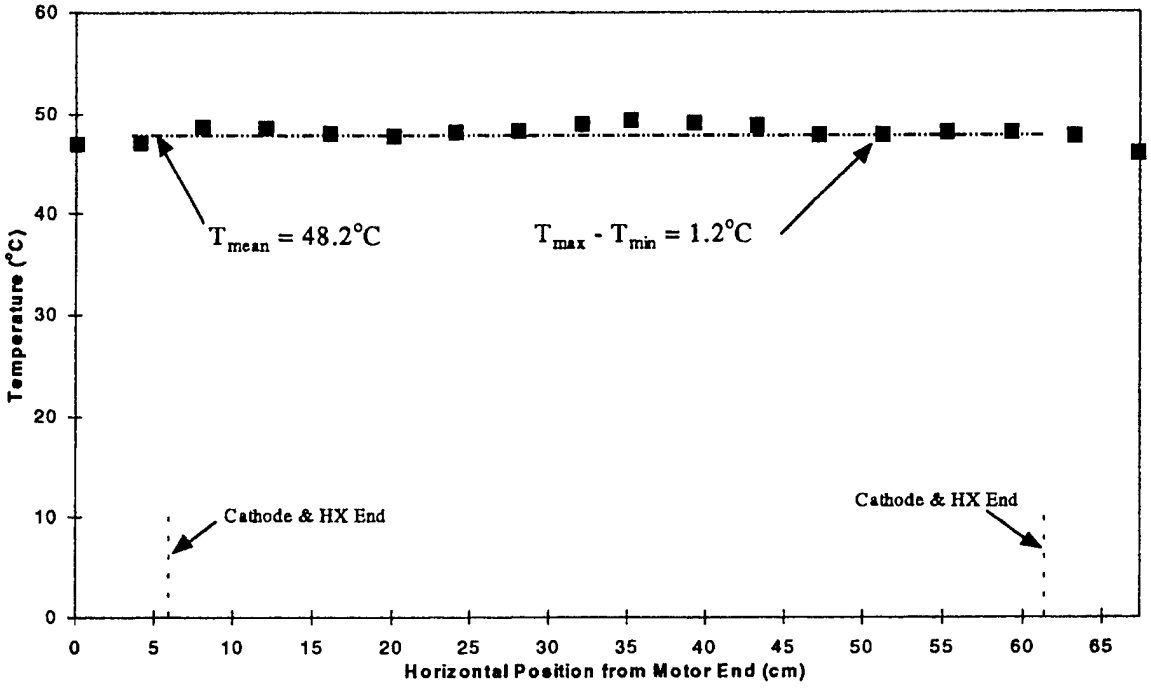

Figure 44. Temperature Profiles along Optical Axis of Brassboard Flow with Heated Air. (Cavity Discharge Height is 16.5 mm)

SRL Brassboard Design Options

The last tasks to be performed under this subcontract have been to test two fan design options. The first feature involves rounding off the leading and trailing edges of the fan blades. Cymer has provided SRL with a fan with these modifications along with a modification of the design of the fan disks at both ends. However, careful examination of the blades shows that leading edges of the some of the blades are rounded while others are squared. Further modifications had to be made to adapt to the existing shaft and coupling design of the Brassboard Flow model The active fan length is the same as the standard "stiffened" fan, used for all the tests thus far and in the SRL Brassboard, however this modified fan is 0.38" shorter. Whether this design option would or would not improve performance could not be evaluated since the fan supplied was not properly fabricated.

Tests have been performed to determine the importance of the under-cut in the sidewall own in Figure 17. The SRL Brassboard was designed and built with this under-cut for the fan to minimize the flow "dead region" and improve flow uniformity along the optics axis.

The last tasks to be performed under this subcontract have been to test two fan design options. The first feature involves rounding off the leading and trailing edges of the fan blades. Cymer has provided SRL with a fan with these modifications along with a modification of the design of the fan disks at both ends. However, careful examination of the blades show that leading edges of the some of the blades are rounded while others are squared. Further modifications had to be made to adapt to the existing shaft and coupling design of the Brassboard Flow modeL The active fan length is the same as the standard "stiffened" fan, used for all the tests thus far and in the SRL Brassboard, however this modified fan is 0.38" shorter. Whether this design option would or would not improve performance could not be evaluated since the fan supplied was not properly fabricated.

Tests have been performed to determine the importance of the under-cut in the sidewall for the fan as shown in Figure 17. The SRL Brassboard was designed and built with this under-cut for the fan to minimize the flow "dead region" and improve flow uniformity along the optical axis. The SRL Brassboard Flow Model also was configured with this feature as shown in Figure 34 for all of the tests reported thus far. The flow model was re-configured to eliminate this under-cut at the bearing end. Test results comparing velocity profiles from the bearing end with and without the under-cut are shown in Figure 45. These show that there is less of a velocity roll-off near the end walls. The mean to minimum velocity, $(U_{mean} - U_{min})/U_{mean}$, is 22.3% with the under-cut compared to 35.2% without the under-cut. Here, $\boldsymbol{U_{min}}$ refers to the minimum velocity over traversed region. Incorporation of the under-cut into the SRL Brassboard design potentially allows a shorter window wall-to-window wall optical length for a given cathode length thereby reducing the total volumetric flow required, and therefore fan power demand.

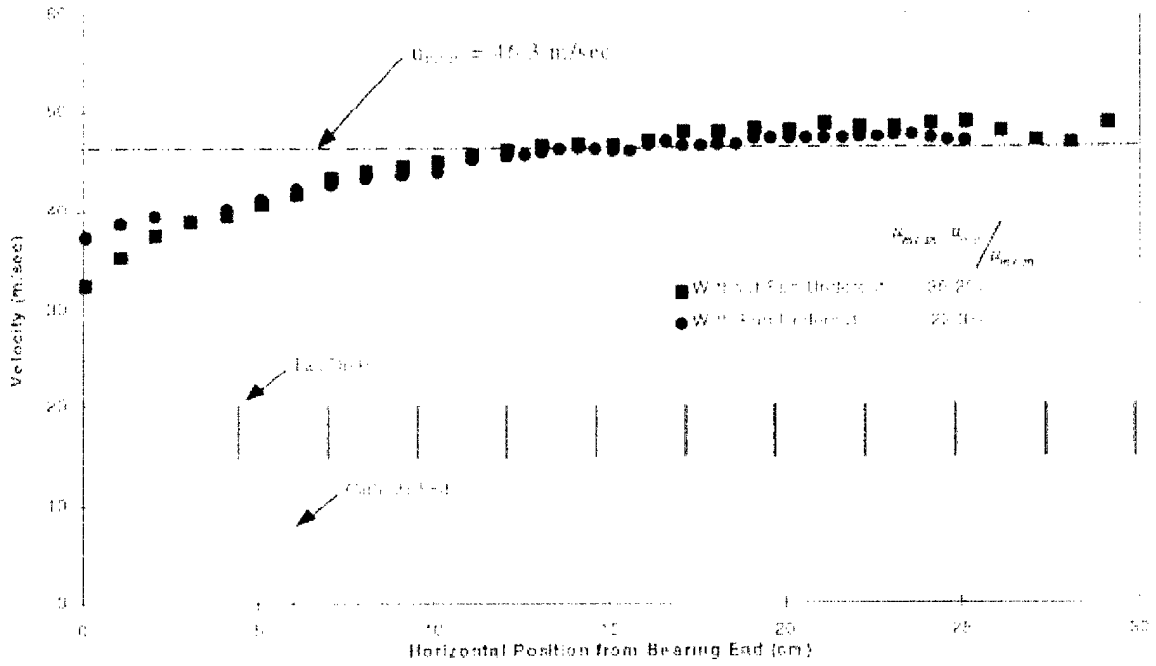

Figure 45. Velocity Profiles along Optical Axis of Brassboard Flow Model with and without Fan Undercut in Sidewalls (Pan Speed at 4800 RPM)

SRL Brassboard Flow Model: Dual Motor Test Results.

The SRL Brassboard Flow Model was configured with dual Cymer motors, as shown in Figure 46. Initially a number of difficulties were encountered with the available motor/motor controller combinations. After a series of tests we concluded that the motor/motor controller pairs need to be well matched if one is to make use of the maximum available motor power. A well matched set of motors and motor controllers were obtained to conclude dual motor tests.

Tests on the SRL Brassboard Flow Model filled with air and $C0_2$, and configured with dual Cymer motors and 220 Vac controllers were performed with the baseline cavity discharge height of 16.5 mm. Test results are shown in Figure 47 and Figure 48. Cavity velocity measurements with dual Cymer motors are similar to those with the single 3 hp motor presented in the previous section. At any given fan speed, cavity gas velocity is somewhat higher with CO_2. The fan power demand with CO_2 was scaled with (divided by) the density ratio ($\sigma = \rho\ CO_2\ \rho_{air} = 1.52$) to obtain the "Air Equivalent" power demand. Figure 47 shows agreement of the air equivalent power demand and the fan power demand for air, as has been demonstrated previously. As expected, fan power demand is significantly higher, and correspondingly efficiency is lower, with dual motors when compared to the single 3 hp motor.

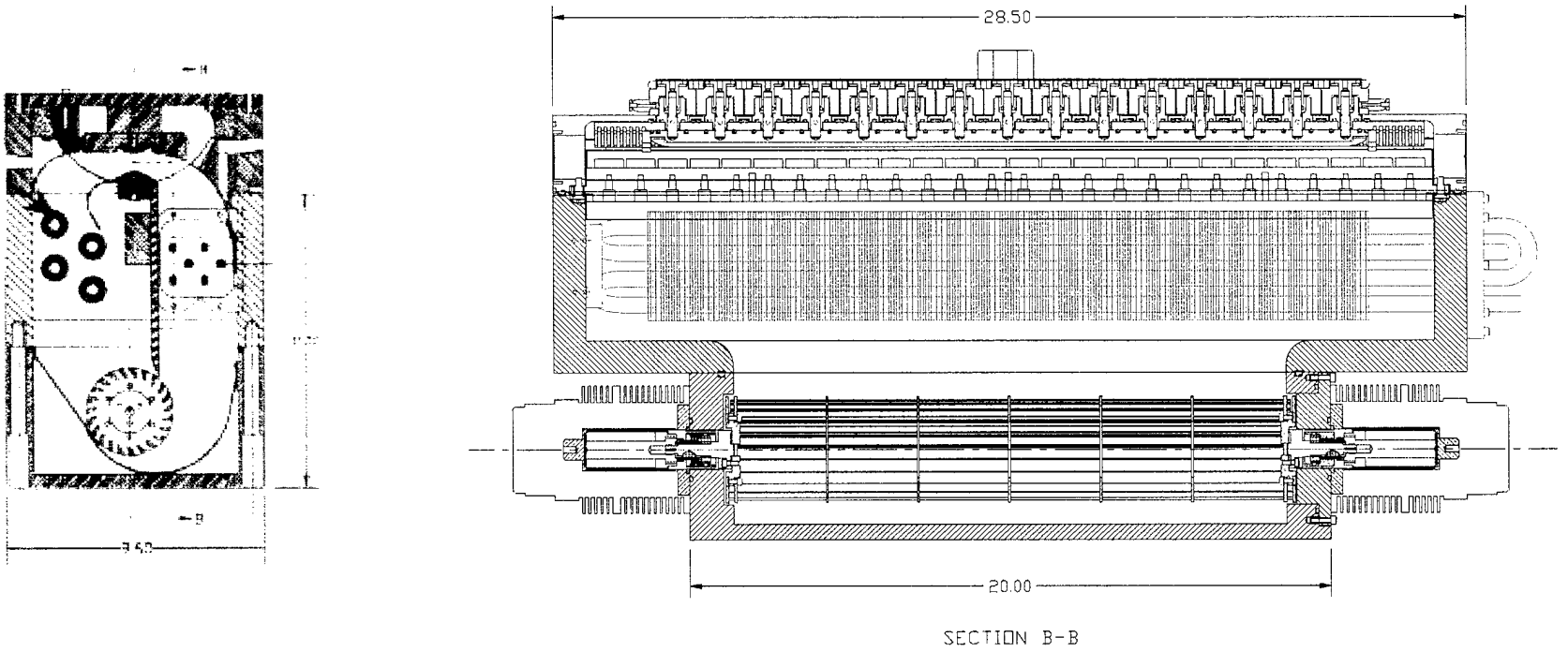

final_fasbihtr report_figures.ppt
9 19 2001

Figure 46. SRL Brassboard Flow Model with Dual Cymer Motors, SRL Heat Exchanger Design, and "Streamlined" Low Inductance Head

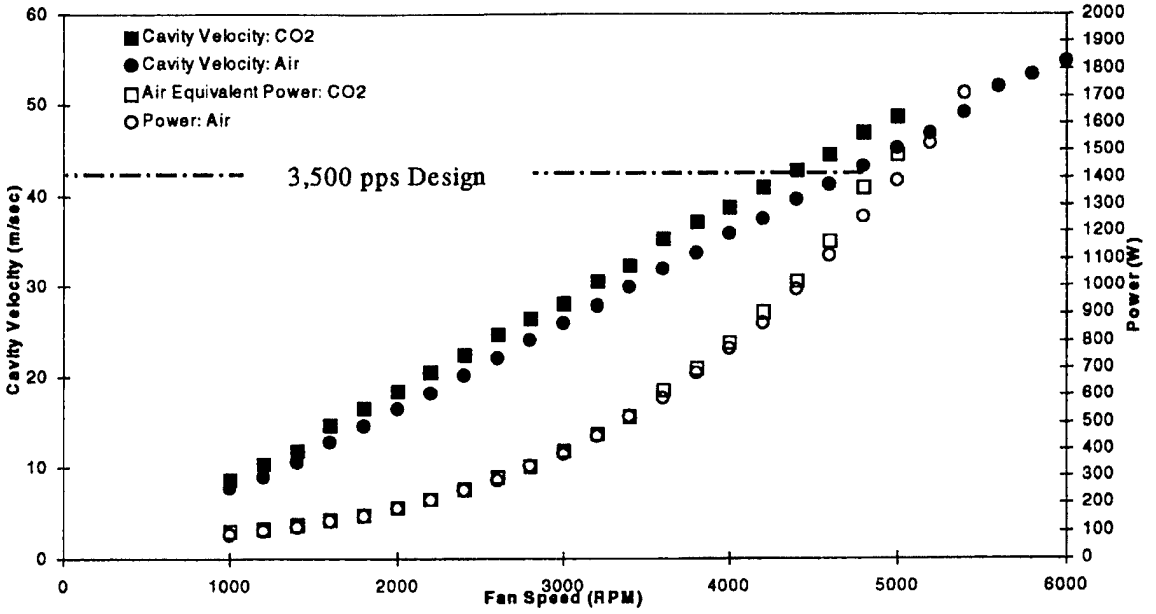

Figure 47. SRL Brassboard Flow Model Test Data: Comparison of Model filled with Air and with CO_2

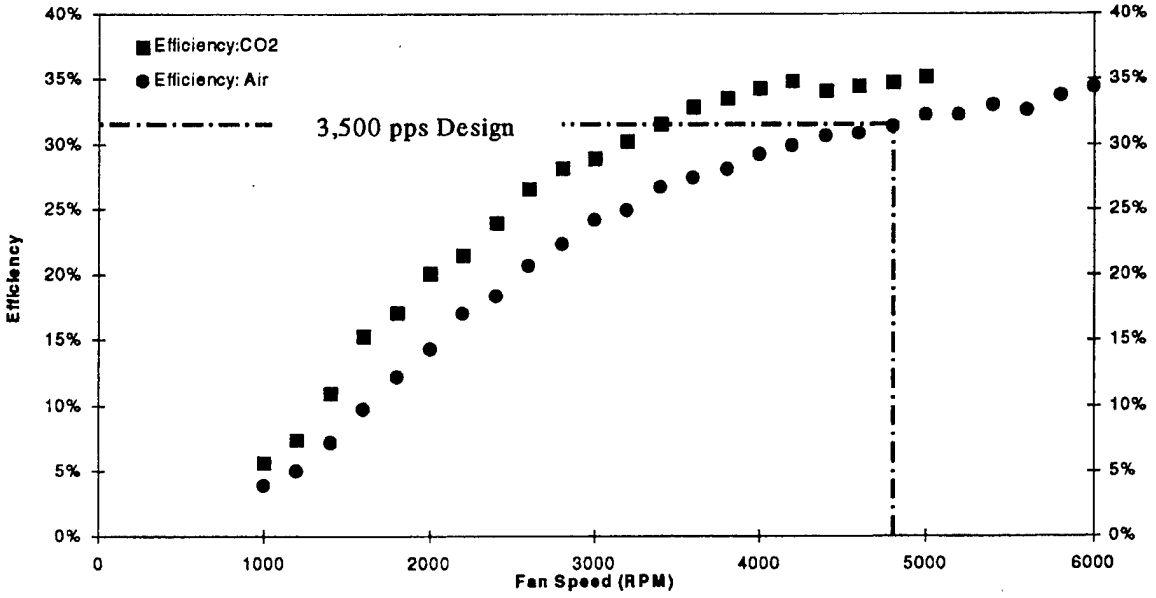

Figure 48. SRL Brassboard Flow Model Fan Efficiency Data: Comparison Model Filled with Air and with CO_2

VII. Brassboard Design

Tests on the Brassboard Design configured with dual Cymer motors and 220 Vac controllers, as shown in Figure 17 and Figure 18, have been performed at Cymer with the baseline cavity discharge height of 16.5 mm. The Brassboard was filled with a Ne/Kr gas mix at three different pressures: 1) P=1 atm., 2) P=1.4, atm. to simulate air tests performed with the flow model and 3) P=3.24 atm. to simulate laser gas density at design pressure and temperature. Test results are compared for the three different pressures and with those of the SRL Brassboard Flow Model filled with air in Figure 49. Testing for a gas pressure of 3.24 atm was limited to a maximum fan speed of 4280 RPM due to a combined maximum fan motor power limitation of 1700 W. At any given fan speed, cavity gas velocity is higher with higher gas density. The fan power demand was scaled with (divided by) the density ratio ($\sigma = \rho_{Ne/Kr}/\rho_{air}$) to obtain the "Air Equivalent" power demand. The test data in Figure 49 shows good agreement with the SRL Brassboard Flow Model test data.

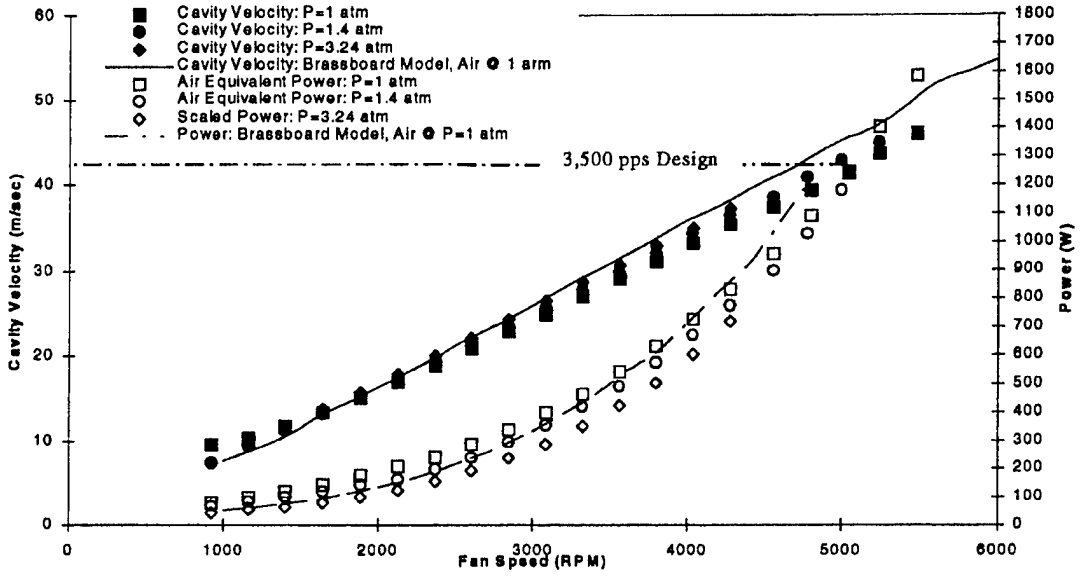

Figure 49. Brassboard Design Test Data: Comparison of Flow System Filled with Ne/Kr Mix at Different Pressures and SRL Brassboard Model Filled with Air.